

EXPERIMENTAL MEASUREMENT OF THE RESPONSE OF CENTRIFUGAL
PENDULUM VIBRATION ABSORBERS

By

Abhisek Jain

A THESIS

Submitted to
Michigan State University
in partial fulfillment of the requirements
for the degree of

Mechanical Engineering - Master of Science

2013

ABSTRACT

EXPERIMENTAL MEASUREMENT OF THE RESPONSE OF CENTRIFUGAL PENDULUM VIBRATION ABSORBERS

By

Abhisek Jain

Centrifugal pendulum vibration absorbers (CPVAs) are devices designed to reduce torsional oscillations in order-excited rotational systems. The focus of this research is to develop and test algorithms that allow one to determine the absorber motion (amplitude and phase) using the readouts from an accelerometer attached to the absorber and an encoder sensing the rotor motion. This requires a detailed analysis of the pendulum kinematics, which depends on the path followed by the absorber mass and the rotation of the absorber relative to the rotor. The absorber kinematics are governed by a differential equation that relates the absolute absorber acceleration (measured signal from an accelerometer) and the rotor speed and acceleration (measured signal from an encoder), to the motion of the absorber relative to the rotor. This differential equation is solved approximately using a harmonic-balance method, based on assumptions regarding the significant harmonics in the rotor and absorber dynamics. The resulting approximations are tested using numerical simulations of the equations of motion, as well as in experiments in which the approximated absorber motions are compared to direct encoder measurements of the response. Both simulations and experiments show that absorber motions are successfully estimated from measurements of the absolute acceleration of the absorber and rotor motions, although some deviation is apparent when absorber motions have large amplitudes. This approach will allow test engineers to validate models that predict and assess absorber performance in rotational systems (e.g., automobile engines), which will improve confidence in the absorber design process.

To my Mom, Dad and Brother.

ACKNOWLEDGMENTS

In my two years of graduate school at Michigan State University, I believe that I have doubled my understanding of dynamics and this would not have been possible without the guidance and support of my advisors, Dr. Steve Shaw and Dr. Brian Feeny. Professor Shaw is an expert in dynamical systems and an amazing advisor. I thoroughly loved working on my project under his guidance and the learning process have been extremely gratifying. Professor Feeny has also been a great mentor for me throughout my research and his expertise has been equally invaluable. I would also like to thank Professor Ranjan Mukherjee for serving on my committee.

Special thanks goes to Brendan Vidmar who was a friend and a teacher for me for almost a year in my graduate studies. He has helped me in understanding the CPVA system and in setting up experiments for my project. The amount of knowledge I have acquired about dynamics comes not only from my research but also from many discussions with Brendan. The undergraduate students who worked in CPVA group also helped me in implementing experimental setup and in conducting experiments. I thank J. T. Whitman, Bara Aldasouqi and Cody Little for their help. I would also like to thank graduate students Scott Strachan, Pavel Polunin, Venkat Ramakrishnan, Xing Xing and Mustafa Ali Acar and undergraduate student Ming Mu for their help and support and also for numerous discussions in the subject of dynamics.

I thank Bruce Geist of Chrysler LLC for his expert comments and discussion during our weekly meetings. He has also helped and guided me in numerous aspects of my project. I also thank Chrysler LLC for machining the experimental absorbers on which all my experiments have been conducted. I thank Jeff Chottiner and Vince Solferino from Ford Motor Company

and Steve Walters and Mark Schrewe from Honda R & D Americas for providing practical experience in CPVA absorbers. I must thank Analog Devices for providing me free samples of their accelerometers used for the experiments in my research. I also thank the ECE shop of MSU for designing the PCB board that was used to mount the accelerometers.

My final thanks goes out to the National Science Foundation (Grant Number CMMI-1100260), which provided funding for this work as well as to Honda R & D Americas for providing financial support for my graduate studies.

TABLE OF CONTENTS

LIST OF TABLES	vii
LIST OF FIGURES	viii
Chapter 1 Introduction	1
1.1 Motivation	2
1.2 Basic Operation of a CPVA	4
Chapter 2 Methods and Results	8
2.1 Kinematic Analysis	8
2.1.1 Absorber Arrangement	9
2.1.1.1 Hinged Circular Path Absorbers	11
2.1.1.2 Bifilar Absorbers	14
2.1.2 Kinematic Differential Equation for the Absorber Response	17
2.1.3 Approximate Kinematic Solutions	18
2.2 Experimental Setup and Methods	26
2.2.1 Experimental Rig	26
2.2.2 Accelerometer Arrangement	27
2.2.3 System Parameter Values	28
2.3 Results	34
2.3.1 Simulations	34
2.3.2 Experimental Results	37
Chapter 3 Conclusions and Future Work	40
APPENDIX	44
BIBLIOGRAPHY	55

LIST OF TABLES

Table 1.1	Acclerometer vs encoder	4
Table 2.1	Parameter Values for Experiments	32
Table 2.2	Parameter Values for Dynamic Simulations [1]	33

LIST OF FIGURES

Figure 1.1	Cycloidal path CPVAs on a helicopter rotor, picture taken by Steve Shaw. For interpretation of the references to color in this and all other figures, the reader is referred to the electronic version of this thesis.	3
Figure 1.2	Circular path CPVA on the crankshaft of a prototype internal combustion engine [2].	3
Figure 1.3	Comparison of a CPVA with a simple pendulum: left: simple pendulum. Right: centrifugal pendulum.	5
Figure 2.1	Hinged circular path absorbers.	9
Figure 2.2	Bifilar absorber arrangement.	10
Figure 2.3	Model of a circular path absorber, hinged at point A . Axis of rotation of rotor is point O , R is the distance between rotor axis O and absorber hinge point A , L is the distance between point A and the absorber path vertex V (equal to the constant pendulum length), point C shows the location of the COM of the absorber, \hat{e}_R is the unit vector normal to the absorber COM path at vertex V and moving with the rotor at $\dot{\theta}$, \hat{e}_θ is the unit vector tangent to the absorber COM path at vertex V , ϕ is the angular displacement of the absorber with respect to the rotor, \vec{r}_c is the position vector of absorber COM measured from point O , \hat{e}_L is the unit vector normal to the absorber COM path at a location which is at an angle ϕ from V and it moves with the absorber at angular speed $(\dot{\theta} + \dot{\phi})$, and \hat{e}_ϕ is the unit vector tangent to the absorber COM path at same location as \hat{e}_L and moves at an angular speed of $(\dot{\theta} + \dot{\phi})$	12
Figure 2.4	Location of accelerometer from COM of a hinged absorber.	13
Figure 2.5	x and y axes fixed to accelerometer frame along which the absolute acceleration is measured.	14

Figure 2.6	Model for a general path bifilar absorber attached to a rotor. Axis of rotation passing through point O (perpendicular to the plane of paper) with COM of absorber at point C , \hat{e}_R and \hat{e}_θ are unit vectors as defined in Figure 2.3, θ is the instantaneous angular displacement of rotor from a reference position, s is the instantaneous distance of the absorber from the vertex V and measured along the path traversed by the COM, V is the vertex of the path, \vec{r}_C is the position vector of absorber COM measured from point O , $X(s)$ is the instantaneous distance of the absorber from the rotor axis O and measured along unit vector \hat{e}_θ , $Y(s)$ is the instantaneous distance of the absorber from the rotor axis O and measured along unit vector \hat{e}_R , and the rectangular box in the figure represents the absorber moving along the specified path.	15
Figure 2.7	Location of accelerometer from COM of a bifilar absorber.	17
Figure 2.8	Experimental rig.	26
Figure 2.9	Closeup of unmounted absorber mass, with accelerometer and encoder.	28
Figure 2.10	Procedure to measure the absorber COM distance from the rotor center.	29
Figure 2.11	Order n amplitude of the rotor angular acceleration divided by the amplitude of fluctuating torque as a function of the applied torque order, n	31
Figure 2.12	Normalized absorber displacement amplitude estimated from linear (Δ) and cubic (\square) analysis compared with exact values (\circ) at 400 RPM, over a range of absorber response amplitudes.	35
Figure 2.13	Normalized absorber displacement amplitude estimated from linear (Δ) and cubic (\square) analyses compared with exact values (\circ) at 300 RPM, over a range of absorber response amplitudes.	35
Figure 2.14	Absorber displacement amplitude S estimated from linear (Δ) and cubic (\square) analyses compared with encoder values (\circ) at 300 RPM.	38
Figure 2.15	Absorber displacement amplitude S estimated from linear (Δ) and cubic (\square) analyses compared with encoder values (\circ) at 400 RPM.	38
Figure 2.16	Absorber displacement amplitude S estimated from linear (Δ) and cubic (\square) analyses compared with encoder values (\circ) at 500 RPM.	39

Figure 2.17	Comparison of cubic estimation from simulations and experiments. .	39
Figure 3.1	Comparison of simulated absorber dynamics with the numerical solution of differential equation (2.8).	42

Chapter 1

Introduction

This study considers the development of a method for experimentally measuring the response of centrifugally driven pendulum vibration absorbers (CPVAs). These absorbers consist of masses suspended from a rotor (hinged or suspended through rollers) such that they are free to oscillate relative to the rotor. When correctly tuned they are capable of reducing machine-order torsional (twisting) vibrations in rotating machinery. These absorbers are currently being developed for automotive engine applications, where reduction of crankshaft torsional vibrations will allow for low-speed, high-torque operation, resulting in significant improvements in fuel economy. The development of these absorbers requires extensive testing, and while it is quite simple to measure rotor torsional vibrations, currently no convenient method exists for determining the motion of the absorbers in a rotating machine. The present work is aimed at developing the tools needed to measure absorber dynamics using an accelerometer fixed to the absorber mass, where the signal can be transmitted via a slip ring or by telemetry [3].

In this chapter we will state the motivation of this research and will later include some background on centrifugal pendulum vibration absorbers. The second chapter contains the theory developed for this research and the validation of the theory with simulations and experiments. The third and final chapter contains conclusions and inferences from this research, and some directions for future work in this area.

1.1 Motivation

CPVAs are devices that reduce undesired torsional vibration in a rotating systems. Torsional vibrations occur in rotors when the torque source is oscillatory in nature. When the torque input to the system is periodic, with frequency proportional to mean speed (known as engine-order excitation), CPVAs can be implemented to absorb the torsional vibrations in the rotor at the problematic order. A typical example of order excitation occurs in an automobile engine, where the excitation arises from cylinder pressure, resulting in an order equal to half the number of cylinders.

A basic CPVA device consists of a rotor and an absorber mass hinged to the rotor. The rotor is free to rotate about its axis and the absorber is restricted to move along a certain path with respect to the rotor. CPVA systems have been researched for several decades [4, 5, 6, 7, 8, 9] and have been implemented in various rotational systems, including helicopter rotors and automobile engines [6, 8, 9, 2, 1]; see Figures 1.1 and 1.2. Once properly designed and implemented, there is no need to measure the response of a CPVA system. However, such measurements are very important during the development of these systems. The rotor dynamics of the CPVA system can be easily measured using encoders. The absorber dynamics can be easily measured using encoders in a laboratory environment if there is ample space, but it is not feasible to implement encoders for absorbers in experiments that are tightly spaced, or in prototype engines and drive trains which may have harsh environments. These issues provide motivation to find alternative ways to measure absorbers in a rotating machine.

The goal of this research is to develop a strategy by which one can conveniently measure the dynamics of these absorbers in running machines such as internal combustion engines.

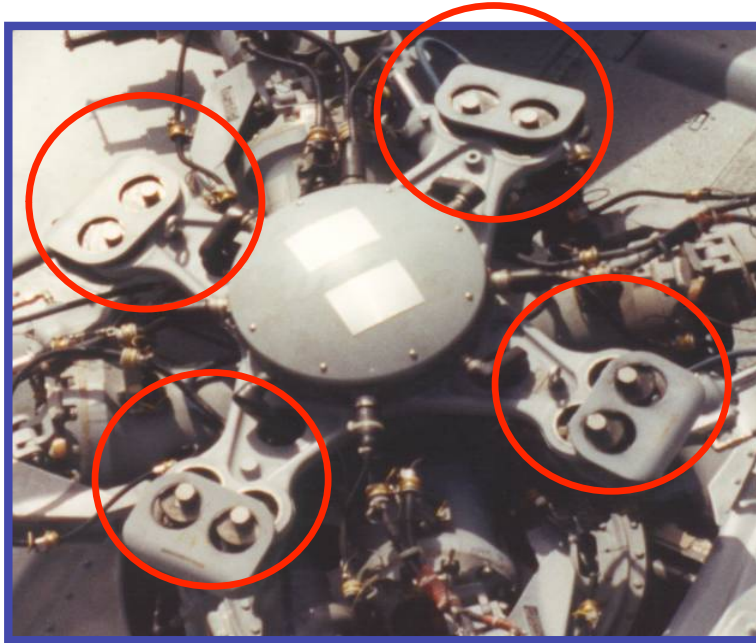


Figure 1.1: Cycloidal path CPVAs on a helicopter rotor, picture taken by Steve Shaw. For interpretation of the references to color in this and all other figures, the reader is referred to the electronic version of this thesis.

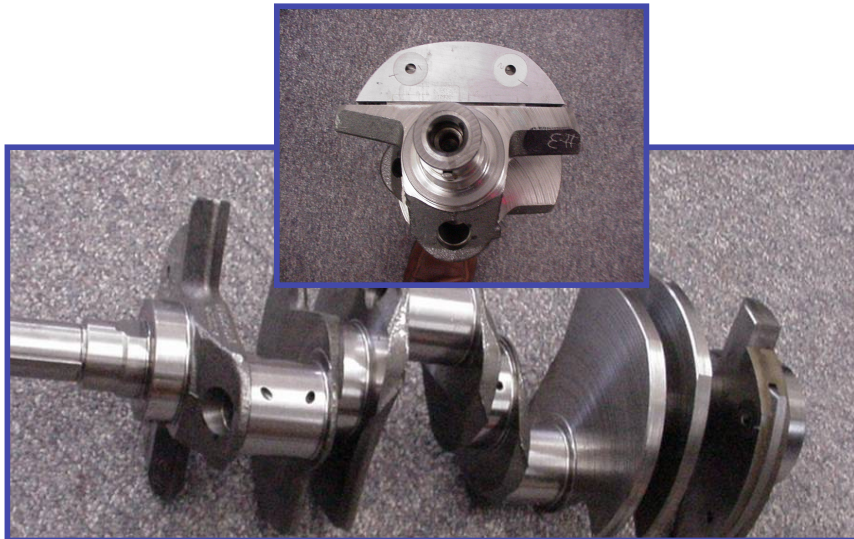


Figure 1.2: Circular path CPVA on the crankshaft of a prototype internal combustion engine [2].

In this research, we develop an analysis method by which one can estimate the dynamics of absorbers using accelerometers fixed to the absorber mass. The benefits and limitations of using accelerometers over encoders are listed in Table 1.1. The idea is to measure the absolute acceleration of the absorber, and also independently measure the rotor dynamics using an encoder (which is already implemented in many rotating systems) and use these measurements to estimate the motion of the absorbers relative to the rotor. The success of this approach will help with the testing of proposed absorber designs, and will also aid in basic research related to these absorbers.

Table 1.1: **Accelerometer vs encoder**

Accelerometer	Encoder
Small size, and mass. Can directly be attached to absorber	Comparatively large, typically attached to rotor and requires extra space and arrangement on absorber
Measurement has to be further processed to determine the absorber dynamics relative to rotor	Provides a direct and independent measurement of absorber dynamics relative to rotor

1.2 Basic Operation of a CPVA

The physical arrangement of a centrifugal pendulum is similar to that of a simple pendulum. However, the restoring force arises from a centrifugal field instead of gravity, as depicted in Figure 1.3.

The left panel of Figure 1.3 shows a simple pendulum with mass P and length L hinged

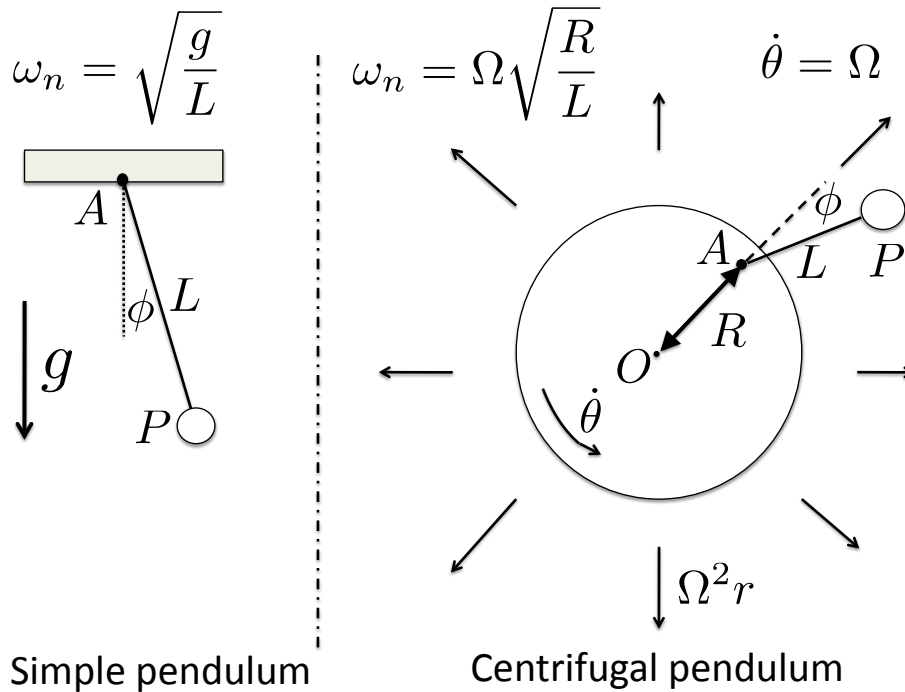


Figure 1.3: Comparison of a CPVA with a simple pendulum: left: simple pendulum. Right: centrifugal pendulum.

with a stationary base at point A . The restoring force for any deviation from the equilibrium position is provided by the gravitational field g , which points downward, and the small amplitude natural frequency of oscillation is $\omega_n = \sqrt{\frac{g}{L}}$. The right panel of Figure 1.3 is that of a centrifugal pendulum with a base rotating about an axis passing through O , perpendicular to the plane of paper, at a constant speed Ω . The pendulum is hinged at a point A to the rotating base, referred to here as the “rotor”. The radially outward arrows show the centrifugal field of magnitude $\Omega^2 r$, r being the radial distance of the point of interest from the rotation axis O . When the rotor is spinning at a constant speed, the equilibrium position of the absorber with respect to the rotor is radially outward. The absorber starts working as soon as there is a disturbance in the mean speed of the rotating system, which arises, for example, from a fluctuation in the applied torque. For small oscillations in angle

ϕ about equilibrium, the linearized natural frequency of the absorber with the rotor spinning at a constant speed Ω is given by

$$\omega_n = \sqrt{\frac{R}{L}}\Omega$$

where R is the distance between the points O and A (see Figure 1.3), and L is the length of the ideal pendulum. The factor $\sqrt{\frac{R}{L}}$ is called the *tuning order* of the absorber and is denoted by \tilde{n} . The term *order* is used to replace frequency in CPVA systems, and it is equal to the number of complete oscillation cycles occurring in each rotor revolution.

This order tuning feature of a centrifugal pendulum is special because it allows the CPVA to operate in reducing engine-order torsional vibrations (defined below) at all rotor speeds. There are a variety of rotational systems where the mean speed of the rotor is variable, and the rotor is subjected to a fluctuating torque that is synchronous with the rotor, resulting in *engine order excitation*, which has frequency $n\Omega$, where n is referred to as the excitation order. If we design the centrifugal pendulum such that its tuning order \tilde{n} is close to n , the pendulum will efficiently absorb vibrations occurring at that order, resulting in lowering the torsional vibration of the rotor at that order [4, 5, 6, 7]. This property makes them highly suitable for a variety of rotating systems, such as internal combustion engines, where the torsional excitation arises from cylinder gas pressure acting through the pistons and connecting rod. For a four stroke engine with N cylinders, the excitation order is $n = \frac{N}{2}$.

In summary, the CPVA system behaves like the classical tuned absorber, with excitation and response focused on a given order (which is fixed for a given machine), rather than a frequency. The dynamics of these absorbers has been studied extensively [5, 6, 7, 8].

Here we focus on a kinematic measurement problem, for which the dynamics are not essential. The basic problem can be viewed from the right panel of Figure 1.3. Of interest is

knowing the pendulum response ϕ relative to the rotor so that the experiments can be used to correlate models and validate analysis, and also to allow the absorber response range to be monitored. Since it is often difficult to measure directly, we develop a method that allows one to compute the relative absorber response ϕ from measurement of the rotor response $\dot{\theta}$ (taken from an encoder) and the absolute acceleration of the pendulum mass P (taken from an accelerometer).

For small amplitude absorber motions this is a linear problem. However, these absorbers are designed to undergo large amplitude oscillations, in which case the kinematics become nonlinear. In fact, the absorbers can be designed so that they follow quite general paths (not just circles) which further complicates the kinematics.

We now turn to the details of this problem and its solutions.

Chapter 2

Methods and Results

In this chapter we develop a theory that will enable us to map the measurements from an accelerometer into absorber response. This mapping will require additional information about the rotor dynamics that can be easily measured using encoders. The analytical approach is developed using basic kinematic relationships, which are then used to derive some convenient approximate expressions for the absorber response. Once the theory is developed, we describe the experimental setup and methodology required to perform experiments. In the third section we show results obtained from simulations and experiments and compare these with the analytical approximations.

2.1 Kinematic Analysis

To develop the model of interest, we assume that the rotor is rigid and spins with fluctuations about a constant mean speed Ω . It is also assumed that the fluctuations in the rotor and the absorber response are periodic. We express the dynamics of the absorber (amplitude and phase) in terms of the absolute acceleration of absorber, the rotor dynamics, and other design parameters. We discuss two different absorber types in section 2.1.1, and describe the models developed for these types in section 2.1.1.1 and section 2.1.1.2, respectively.

2.1.1 Absorber Arrangement

Based on their means of attachment to the rotor, the absorbers can be categorized in two ways: i) single-point hinged compound pendulums (mainly for circular path absorbers) as shown in Figure 2.1 and, ii) two-point suspensions using rollers, also called the bifilar arrangement, as shown in Figure 2.2. For each type it is assumed that the accelerometer is fixed to the absorber mass, so that the accelerations measured are two components of its absolute acceleration oriented with the absorber.

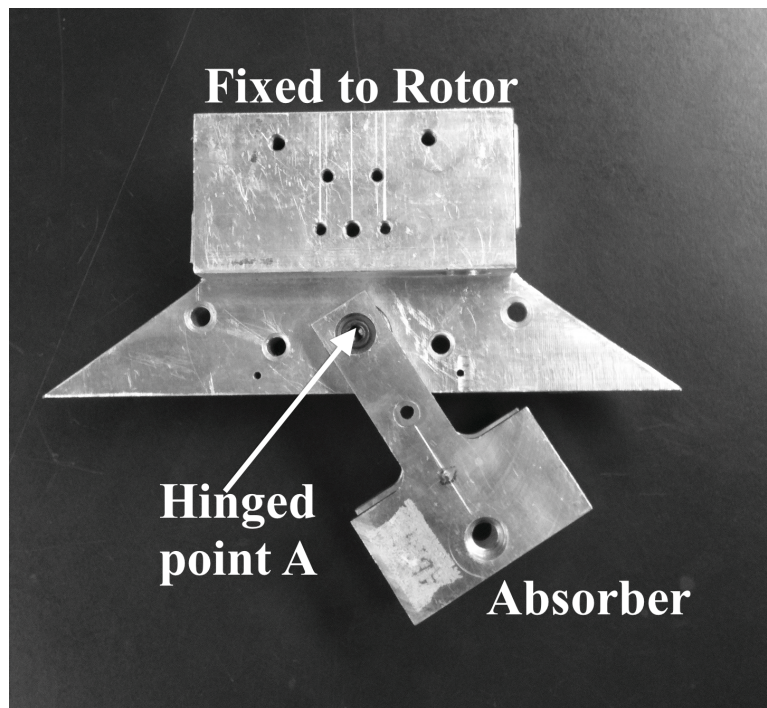


Figure 2.1: Hinged circular path absorbers.

A compound pendulum pivoted about a fixed point (point A in Figure 2.1) on the absorber is called a single-point hinged absorber. Due to the construction of these absorbers, the path traversed by the center of mass (COM) of these absorbers relative to the rotor is a circle and the absorber body undergoes a rotational motion relative to the rotor. Because of this rotation, an accelerometer (see Figure 2.5) fixed to the absorber will measure its

absolute acceleration along a coordinate system fixed to the absorber. These absorber fixed coordinates (discussed in section 2.1.1.1) will be selected as per convenience.

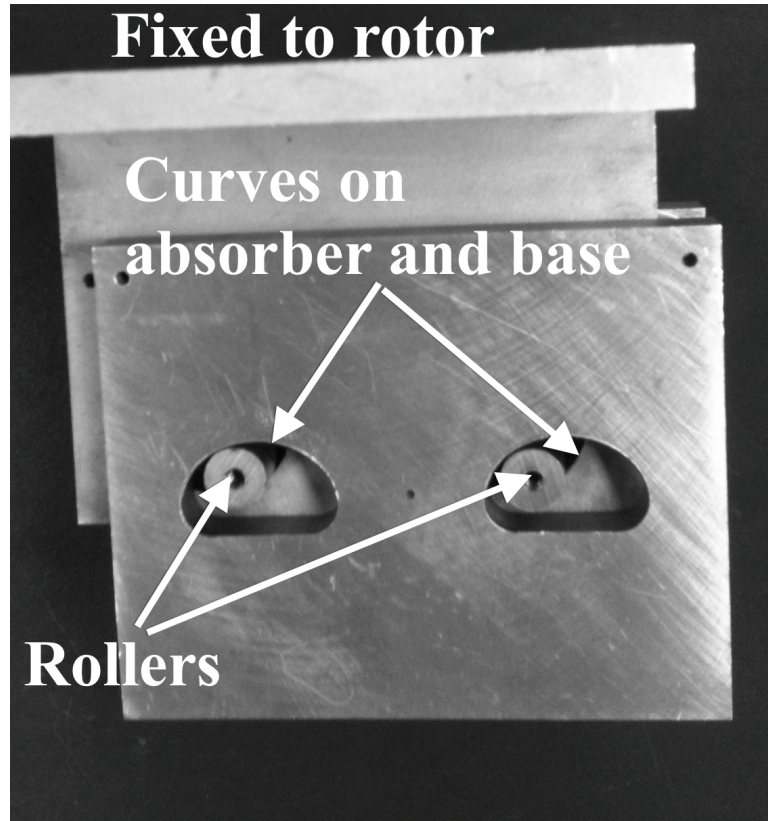


Figure 2.2: Bifilar absorber arrangement.

A bifilar absorber is a compound pendulum restricted at two distinct points (either on a moving base, such as the rotor, or on a base fixed to ground) in such a way that the COM of the pendulum moves along a specific path with respect to the base (see Figure 2.2). Typically, these absorbers are supported using a pair of rollers, as shown in Figure 2.2. Here the absorber and the base each have identical but inverted cutout curves between which cylindrical rollers are placed (see Figure 2.2). The rollers are assumed to roll without slip. The constraint between the absorber and the base makes the COM of the absorber move along a desired path with respect to the base, the path itself prescribed by the design of the cutout curves. This arrangement of the absorber makes the motion of the absorber with

respect to its base purely translational, i.e., it does not rotate relative to the base (in contrast with the hinged absorber). This fact implies that the directions along which the axes of the accelerometer (see Figure 2.5) will be aligned are fixed relative to both the rotor and the absorber. This bifilar arrangement provides a convenient way to construct a general path along which the absorbers are allowed to move relative to the rotor. Bifilar absorbers are most often used in practice. In fact, the absorbers shown in Figure 1.1 and 1.2 are bifilar.

The goal of this effort is to develop a method for both bifilar and hinged arrangements. An analytical approach is formulated and approximate solutions are developed for both types of absorbers. The method developed for bifilar epicycloid path absorbers is experimentally verified.

2.1.1.1 Hinged Circular Path Absorbers

Figure 2.3 shows a schematic model of a hinged type absorber. The caption in Figure 2.3 defines the parameters noted in the figure. Angles θ and ϕ are the degrees of freedom of the absorber-rotor system, ϕ being the absorber coordinate measured relative to a line rotating with the rotor, which we are interested in estimating, and θ being the rotor angle. For convenience, the x and y axes of the accelerometer (shown in Figure 2.5) are assumed to be aligned with unit vectors $\hat{\mathbf{e}}_\phi$ and $\hat{\mathbf{e}}_L$, respectively, from Figure 2.3. The position vector $\vec{\mathbf{r}}_a$ of any general point on the pendulum mass (shown in Figure 2.3) can be written as

$$\vec{\mathbf{r}}_a = \vec{\mathbf{r}}_c + \delta_x \hat{\mathbf{e}}_\phi + \delta_y \hat{\mathbf{e}}_L \quad (2.1)$$

where δ_x and δ_y are the offsets from the COM to the point of interest; see Figure 2.4.

Differentiating $\vec{\mathbf{r}}_a$ in equation (2.1) twice with respect to time, we obtain acceleration

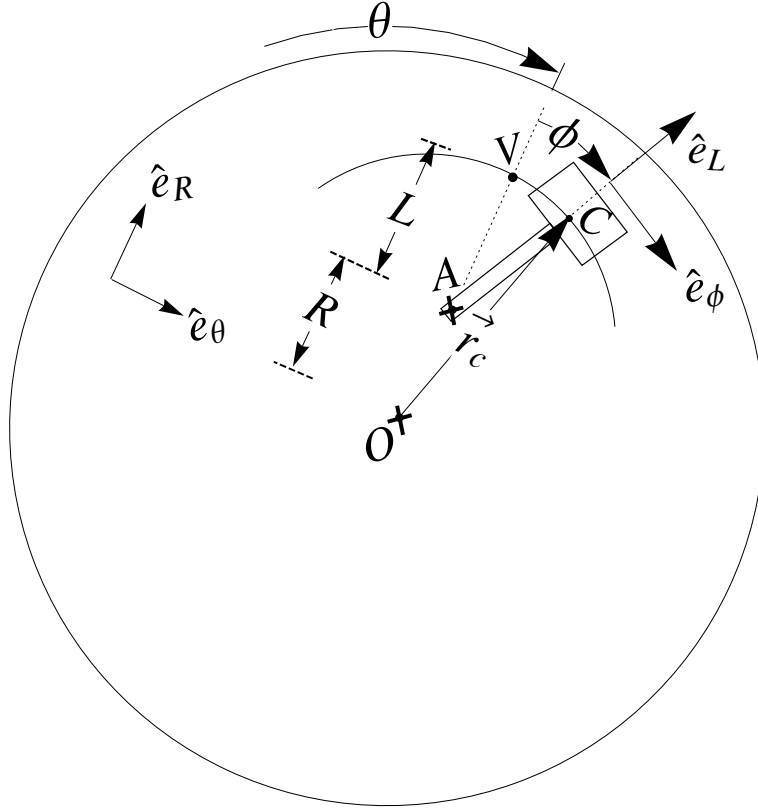


Figure 2.3: Model of a circular path absorber, hinged at point A . Axis of rotation of rotor is point O , R is the distance between rotor axis O and absorber hinge point A , L is the distance between point A and the absorber path vertex V (equal to the constant pendulum length), point C shows the location of the COM of the absorber, \hat{e}_R is the unit vector normal to the absorber COM path at vertex V and moving with the rotor at $\dot{\theta}$, \hat{e}_θ is the unit vector tangent to the absorber COM path at vertex V , ϕ is the angular displacement of the absorber with respect to the rotor, \vec{r}_c is the position vector of absorber COM measured from point O , \hat{e}_L is the unit vector normal to the absorber COM path at a location which is at an angle ϕ from V and it moves with the absorber at angular speed $(\dot{\theta} + \dot{\phi})$, and \hat{e}_ϕ is the unit vector tangent to the absorber COM path at same location as \hat{e}_L and moves at an angular speed of $(\dot{\theta} + \dot{\phi})$.

\vec{a} of this point on the absorber as

$$\vec{a} = R \left(\ddot{\theta} \hat{e}_\theta - \dot{\theta}^2 \hat{e}_R \right) - \delta_x \left((\ddot{\theta} + \ddot{\phi}) \hat{e}_L + (\dot{\theta} + \dot{\phi})^2 \hat{e}_\phi \right) + (L + \delta_y) \left((\ddot{\theta} + \ddot{\phi}) \hat{e}_\phi - (\dot{\theta} + \dot{\phi})^2 \hat{e}_L \right) \quad (2.2)$$

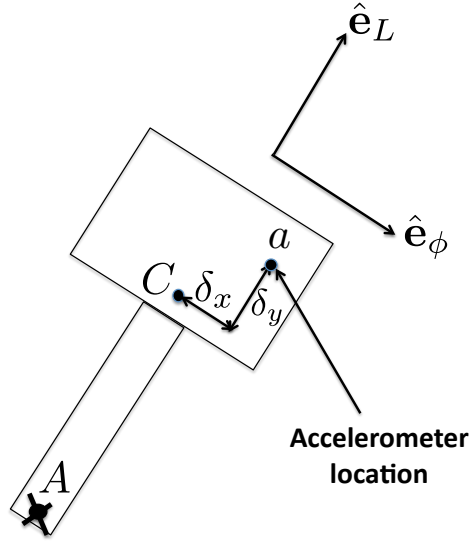


Figure 2.4: Location of accelerometer from COM of a hinged absorber.

The acceleration expression in equation (2.2) needs to be expressed in terms of the unit vectors corresponding to the absorber fixed axes, namely, \hat{e}_L and \hat{e}_ϕ . Using the following transformation from unit vector pair \hat{e}_R and \hat{e}_θ

$$\hat{e}_R = \hat{e}_L \cos \phi - \hat{e}_\phi \sin \phi$$

$$\hat{e}_\theta = \hat{e}_L \sin \phi + \hat{e}_\phi \cos \phi$$

we obtain

$$\vec{a} = a_\phi \hat{e}_\phi + a_L \hat{e}_L \quad (2.3)$$

where

$$a_\phi = R \left(\ddot{\theta} \cos \phi + \dot{\theta}^2 \sin \phi \right) + (L + \delta_y) \left(\ddot{\theta} + \ddot{\phi} \right) - \delta_x \left(\dot{\theta} + \dot{\phi} \right)^2 \quad (2.4)$$

$$a_L = R \left(\ddot{\theta} \sin \phi - \dot{\theta}^2 \cos \phi \right) - (L + \delta_y) \left(\dot{\theta} + \dot{\phi} \right)^2 - \delta_x \left(\ddot{\theta} + \ddot{\phi} \right) \quad (2.5)$$

The expression of the acceleration in equation (2.3) will be used for estimating the relative absorber angle ϕ in terms of other measured quantities, as discussed in section 2.1.3. Now we derive a similar expression for the bifilar arrangement of absorbers.

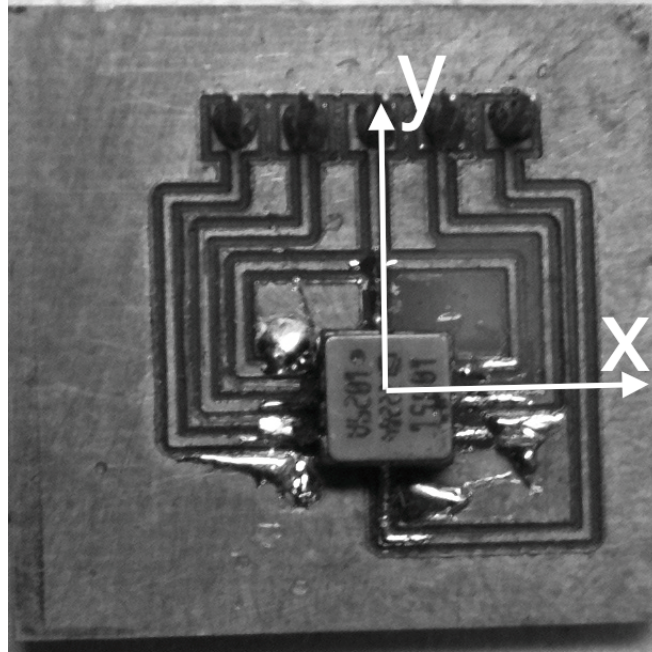


Figure 2.5: x and y axes fixed to accelerometer frame along which the absolute acceleration is measured.

2.1.1.2 Bifilar Absorbers

Figure 2.6 shows a schematic model for a bifilar absorber, where the rectangular box in Figure 2.6 represents the absorber with its COM at point A . The rotor rotates about the

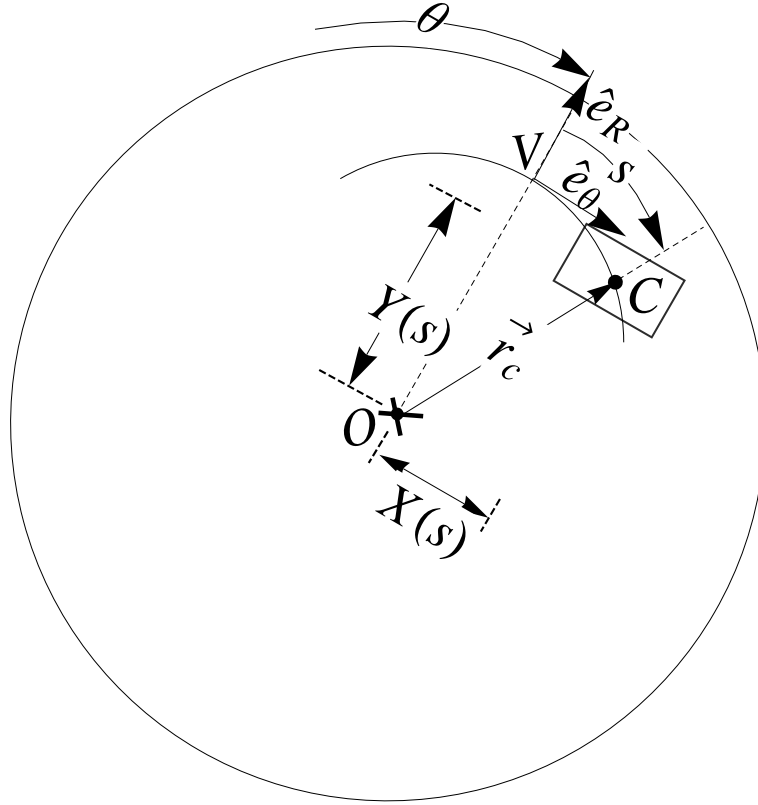


Figure 2.6: Model for a general path bifilar absorber attached to a rotor. Axis of rotation passing through point O (perpendicular to the plane of paper) with COM of absorber at point C , \hat{e}_R and \hat{e}_θ are unit vectors as defined in Figure 2.3, θ is the instantaneous angular displacement of rotor from a reference position, s is the instantaneous distance of the absorber from the vertex V and measured along the path traversed by the COM, V is the vertex of the path, \vec{r}_c is the position vector of absorber COM measured from point O , $X(s)$ is the instantaneous distance of the absorber from the rotor axis O and measured along unit vector \hat{e}_θ , $Y(s)$ is the instantaneous distance of the absorber from the rotor axis O and measured along unit vector \hat{e}_R , and the rectangular box in the figure represents the absorber moving along the specified path.

axis passing through point O . The parameters for the model are defined in the caption of Figure 2.6. Coordinates θ and s represent the two degrees of freedom of this absorber-rotor system. The functions $X(s)$ and $Y(s)$ for a useful class of paths that includes circles, cycloids, and epicycloids can be found in [6]. Note that $\hat{\mathbf{e}}_R$ and $\hat{\mathbf{e}}_\theta$ are, for convenience, taken to be the directions along which the axes (x and y) of the accelerometer are aligned (see Figure 2.5).

The position vector of any general point on such an absorber can be written in terms of $\hat{\mathbf{e}}_R$ and $\hat{\mathbf{e}}_\theta$ as

$$\vec{\mathbf{r}}_a = \vec{\mathbf{r}}_c + \delta_x \hat{\mathbf{e}}_\theta + \delta_y \hat{\mathbf{e}}_R \quad (2.6)$$

where δ_x and δ_y are offsets from the COM to the point of interest; see Figure 2.7.

Differentiating equation (2.6) with respect to time twice, we obtain the acceleration of the point as follows

$$\vec{\mathbf{a}} = a_\theta \hat{\mathbf{e}}_\theta + a_R \hat{\mathbf{e}}_R \quad (2.7)$$

where

$$a_\theta = \left(\ddot{X} - (X + \delta_x) \dot{\theta}^2 + 2 \dot{Y} \dot{\theta} + (Y + \delta_y) \ddot{\theta} \right) \quad (2.8)$$

$$a_R = \left(\ddot{Y} - 2 \dot{X} \dot{\theta} - (X + \delta_x) \ddot{\theta} - (Y + \delta_y) \dot{\theta}^2 \right) \quad (2.9)$$

where, by the chain rule,

$$\begin{aligned} \dot{X} &= \frac{dX}{ds} \dot{s} \\ \ddot{X} &= \frac{d^2X}{ds^2} \dot{s}^2 + \frac{dX}{ds} \ddot{s} \\ \dot{Y} &= \frac{dY}{ds} \dot{s} \\ \ddot{Y} &= \frac{d^2Y}{ds^2} \dot{s}^2 + \frac{dY}{ds} \ddot{s} \end{aligned} \quad (2.10)$$

Equation (2.7) provides an expression which relates measured variables (a_R , a_θ , $\dot{\theta}$, $\ddot{\theta}$) to desired absorber response, expressed as s , through the specified path functions ($X(s)$, $Y(s)$).

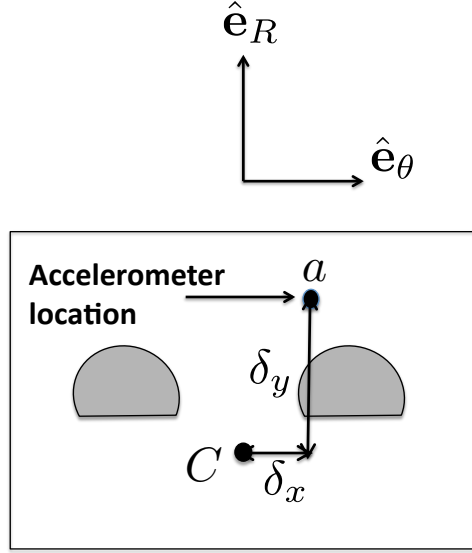


Figure 2.7: Location of accelerometer from COM of a bifilar absorber.

2.1.2 Kinematic Differential Equation for the Absorber Response

Equations (2.3) - (2.5), and equations (2.7) - (2.10), define differential equations in terms of the unknown variables ϕ and s , respectively, with coefficients involving a_ϕ , a_L , $\dot{\theta}$, $\ddot{\theta}$, δ_x , δ_y , L and R for hinged absorbers, and a_θ , a_R , $\dot{\theta}$, $\ddot{\theta}$, δ_x , δ_y and the path parameters for bifilar absorbers. The known coefficients such as a_i measured from accelerometers, θ measured from rotor encoders and the time independent parameters can directly be substituted into the differential equations (2.3) and (2.7). These second-order differential equations are strongly nonlinear and have several time-periodic terms that arise from the measured acceleration and rotor responses. Finding the desired time-periodic solution of these equations is the central

problem of the analysis. One could use numerical techniques (e.g., shooting methods) for their solution. However, it is convenient to have approximate analytical expressions for the time-periodic response. Thus we use a harmonic balance method to solve (2.3) and (2.7), and for this we require some modifications of these equations. This will be developed in section 2.1.3. We will further discuss solutions of the differential equations (2.3) and (2.7) in the last chapter of this thesis.

2.1.3 Approximate Kinematic Solutions

If an accelerometer is fixed on the absorber and the rotating system is in motion, the accelerometer will provide time signals of the absorber acceleration components in directions $\hat{\mathbf{e}}_L$ and $\hat{\mathbf{e}}_\phi$ (Figure 2.3) for hinged absorbers, and $\hat{\mathbf{e}}_R$ and $\hat{\mathbf{e}}_\theta$ (Figure 2.6) for bifilar absorbers. An encoder attached to the rotor will provide $(\dot{\theta}, \ddot{\theta})$ by standard differentiation methods in MATLABTM or LabViewTM. In the present analysis, we intend to measure the absorber and rotor dynamics at steady state, i.e., when the fluctuation over the mean rotor speed is periodic, and the absorber response is periodic. The various assumptions taken in transforming the expressions for the acceleration are as follows (detailed justifications follow below):

- (a) The oscillatory contribution to the acceleration is more useful in the $\hat{\mathbf{e}}_\phi$ and $\hat{\mathbf{e}}_\theta$ components, for the hinged and bifilar absorbers, respectively, than the $\hat{\mathbf{e}}_L$ and $\hat{\mathbf{e}}_R$ components.
- (b) The nonlinear terms can be approximated by expansions to cubic degree in the absorber response coordinates ϕ and s .

(c) For a single harmonic excitation order, the rotor response is represented by three significant harmonics, and the absorber response consists of a single significant harmonic.

The justifications for these assumptions are detailed below.

Regarding assumption (a), the expressions for the acceleration given in equation (2.3) and equation (2.7) consist of two components that are orthogonal to each other, but as per assumption (a) only one of these components is needed to determine the absorber dynamics. In fact, the radial components $\hat{\mathbf{e}}_L$ and $\hat{\mathbf{e}}_R$ are dominated by centripetal effects (represented in the $(R+L)\dot{\theta}^2$ and $Y(s)\dot{\theta}^2$ terms) and are thus less useful for measurement of the absorber motion, since one would have to consider a small oscillation riding on a signal with a large mean value. Thus we consider the $\hat{\mathbf{e}}_\phi$ and $\hat{\mathbf{e}}_\theta$ components of acceleration a_ϕ and a_θ , for hinged and bifilar absorbers, respectively, to estimate the absorber dynamics.

To simplify the expression of the acceleration as per assumption (b), we Taylor expand the path functions. For a hinged absorber we expand $\sin \phi$ and $\cos \phi$ in terms of ϕ , as follows:

$$\begin{aligned}\sin \phi &= \phi - \frac{\phi^3}{3!} + \dots \\ \cos \phi &= 1 - \frac{\phi^2}{2!} + \dots\end{aligned}\tag{2.11}$$

For bifilar absorbers we expand X and Y in terms of s , making use of the fact that the curve followed by the absorbers is symmetric about $X = 0$, so that the expansions take the following form

$$\begin{aligned}X &= \delta_x + X_1 s + X_3 s^3 + \dots \\ Y &= \delta_y + Y_0 + Y_2 s^2 + \dots\end{aligned}\tag{2.12}$$

where the values of the coefficients X_i and Y_i depend on the geometry of the absorber path, and we have again assumed that the accelerometer is installed at position (δ_x, δ_y) from the absorber COM. Coefficients X and Y for various paths can be found in [6]. We substitute these expansions of equations (2.11) and (2.12) into the acceleration coefficients of $\hat{\mathbf{e}}_\phi$ and $\hat{\mathbf{e}}_\theta$ given in equation (2.3) and equation (2.7), respectively, and using assumption (b) we obtain expressions for a_ϕ and a_θ as

$$a_\phi \cong (R + L + \delta_y) \ddot{\theta} + (L + \delta_y) \ddot{\phi} - \delta_x (\dot{\theta} + \dot{\phi})^2 + R\dot{\theta}^2 \left(\phi - \frac{\phi^3}{3!} \right) - R\ddot{\theta} \frac{\phi^2}{2!} \quad (2.13)$$

$$a_\theta \cong X_1 \ddot{s} - (X_1 s + \delta_x) \dot{\theta}^2 + (Y_0 + \delta_y) \ddot{\theta} + (6X_3 s \dot{s} + 4Y_2 s \dot{\theta}) \dot{s} + \left(3X_3 \ddot{s} + Y_2 \ddot{\theta} - X_3 s \dot{\theta}^2 \right) s^2 \quad (2.14)$$

where we note that $\dot{\theta} = \Omega + \Psi(t)$ will have a DC (mean) component of Ω , the mean rotor speed, plus oscillations $\Psi(t)$, and all other time-varying terms will be oscillatory with zero mean. Equations (2.13) and (2.14) are simplified versions of exact differential equations (2.3) and (2.7). The main results of the analysis are obtained by doing a balance of the order n harmonics in these equations. For small amplitudes, the linear truncation may be sufficient, and we also make use of it for comparison purposes, and to determine the limitations of the linearized analysis. The cubic truncations in equations (2.13) and (2.14) are useful for capturing nonlinear kinematic effects of the paths at moderate amplitudes.

Regarding assumption (c), the torque acting on the rotor in the cases of interest is composed of mean and periodic components, with frequencies proportional to the mean speed Ω . If n is the fundamental order of this excitation, the torque can be expressed as

$$T \cong T_0 + \sum_{k=1}^N \left(T_k e^{ikn\Omega t} + T_k^* e^{-ikn\Omega t} \right)$$

where k 's allow for multiple harmonics, and the complex conjugate of T is indicated by T^* . Note that these torques arise from loads that depend on the rotor angle θ , and are then approximated by a Fourier series in which $\theta \approx \Omega t$ is assumed. In general, the torque is dominated by a single order and thus using assumption (c) we claim that the rotor response, represented by $\dot{\theta}$, is dominated by its mean component plus three harmonics. In complex form the rotor speed can be expressed as

$$\dot{\theta} \cong \Omega + \sum_{k=1}^3 \left(Q_k e^{ikn\Omega t} + Q_k^* e^{-ikn\Omega t} \right) \quad (2.15)$$

where the complex conjugate of Q is indicated by Q^* . Note that the harmonic amplitudes Q_k will be determined from measurements of the rotor response.

Similarly, it is observed in simulations and experiments that the absorber response is dominated by a single harmonic at order n [7, 10, 11]. The absorber response is therefore approximated by the following expressions, for hinged and bifilar absorbers, respectively:

$$\phi \cong P e^{in\Omega t} + P^* e^{-in\Omega t} \quad (2.16)$$

$$s \cong S e^{in\Omega t} + S^* e^{-in\Omega t} \quad (2.17)$$

It is the goal of this study to determine complex coefficients P and S from more easily measured quantities, namely, the rotor harmonics, typically obtained from an encoder, and the accelerometer output.

Since the absorber response is dominated by a single harmonic (order n), for each type of absorber only two unknowns are of interest, namely, the real and imaginary parts of P or S , or, equivalently, the amplitude and phase of the order n component of the absorber response. Thus, only two equations are needed to obtain expressions for these unknowns. This allows us to consider only the first harmonic of the series expressions for the acceleration components, which can be expressed as,

$$a_\phi \cong \Phi_1 e^{in\Omega t} + \Phi_1^* e^{-in\Omega t} \quad (2.18)$$

$$a_\theta \cong \Theta_1 e^{in\Omega t} + \Theta_1^* e^{-in\Omega t} \quad (2.19)$$

Harmonic assumptions (2.16 - 2.19) are inserted into equations (2.13) and (2.14), which are then expanded in terms of their harmonic components. The equations to be solved for the unknowns P and S are obtained by retaining only the first harmonic of the resulting expansion, resulting in a pair of equations for the real and imaginary parts of P and S . It is important to note that due to nonlinear kinematic effects, harmonics will couple to one another, resulting in equations that involve order n harmonics from all sources, as well as higher order harmonic coefficients from the rotor response. These equations are detailed in Appendix A, specifically equations (A.12 - A.13) for hinged absorbers and equations (A.44 - A.45) for bifilar absorbers. Each set of equations is a pair of coupled cubic equations in the unknown coefficients, and therefore they cannot be solved in closed form. If one retains

only linear terms, the equations become two linear equations in two unknowns which can be inverted in closed form. For solving the equations for the unknowns of interest, P and S , the following information is used: The harmonic coefficient Φ_1 or Θ_1 is determined from a Fourier analysis of the signal from the accelerometer; quantities Q_k and Ω are determined from a Fourier analysis of the measured rotor response; and the excitation order n and system geometric variables are known from the physical configuration of the system.

In the following section, we demonstrate results for a bifilar absorber system using three levels of approximation. The first is the linear approximation, which can be solved in closed form; the second is the cubic approximation, which requires the solution of the polynomial equations given in Appendix A and B; the third approximation comes from direct simulation of the system dynamic equations, which are labeled as “exact”. The closed form solution for linear approximations will be discussed here.

If we linearize the expressions for a_ϕ and a_θ in equations (2.13) and (2.14) and substitute the harmonic expansions given in equations (2.15 - 2.17), we obtain expressions for Φ_1 and Θ_1 , respectively, that are linear in terms of the absorber amplitudes P and S . Expressing Φ_1 and P in terms of real and imaginary parts, with the subscripts “r” and “i”, respectively, and inverting the expressions, yields

$$\begin{aligned} P_r &= \frac{(\Phi_r - c_1) f_4 - (\Phi_i - c_2) f_2}{f_1 f_4 - f_2 f_3} \\ P_i &= \frac{(\Phi_r - c_1) f_3 - (\Phi_i - c_2) f_1}{f_2 f_3 - f_4 f_1} \end{aligned} \tag{2.20}$$

where f_1, f_2, f_3, f_4, c_1 and c_2 are expressions of known variables and measured quantities (see Appendix (A.1.1) for expression for the f_i 's and $c_{1,2}$).

Doing the same for Θ_1 and S , we find

$$\begin{aligned} S_r &= \frac{(\Theta_r - C_1) F_4 - (\Theta_i - C_2) F_2}{F_1 F_4 - F_2 F_3} \\ S_i &= \frac{(\Theta_r - C_1) F_3 - (\Theta_i - C_2) F_1}{F_2 F_3 - F_4 F_1} \end{aligned} \quad (2.21)$$

where F_1, F_2, F_3, F_4, C_1 and C_2 are expressions of known variables and measured quantities (see Appendix (A.2.1) for expressions for the of F_j 's and $C_{1,2}$).

Equations (2.20) and (2.21) provide closed-form approximate solutions for the real and imaginary parts of the absorber response, from which the amplitude and phase can be determined. These expressions have linear relationships between the acceleration component of interest and the absorber complex amplitude. However, in order to consider a range of response amplitudes for the dynamic system, one varies the amplitude of the fluctuating torque applied to the rotor, denoted here by Γ , and the absorber and accelerometer responses are nonlinear in terms of Γ . Therefore, when one plots results for the absorber amplitude obtained from the linear approximation, the curve will be linear if plotted versus the acceleration component, but nonlinear if plotted versus Γ . In our study we vary Γ , since this corresponds to what is done when investigating the system dynamics.

While the linear approximation yields convenient (if lengthy) closed form expressions, more accurate approximations can be obtained by considering nonlinear relationships. A first step in this direction is to use the cubic approximations given in equations (2.13) and (2.14). Applying the harmonic approximations to these equations leads to polynomial (coupled cubic) equations for P_r and P_i for hinged absorbers, and for S_r and S_i for bifilar absorbers. These equations, which are given in Appendix A.2.2, cannot be solved in closed form, and therefore numerical solutions are required. It is found that these cubic approximations

improve the accuracy of the results when compared to the linear approximations, but the gain is generally not worth the increased complexity in the equations.

If one is going to use numerical methods, it is suggested that the kinematic differential equations for a_ϕ (given in equation (2.4)) or a_θ (given in equation (2.8)) be solved by more direct methods. These expressions do not involve any approximations, but they require numerical solution of a differential equation with unknown initial conditions. Specifically, one would feed into these equations data from the accelerometer and rotor encoder (in the form of harmonic amplitudes and phases), and seek the periodic solution for ϕ for hinged absorbers, or for S for bifilar absorbers (recalling in the latter case that X and Y are functions of S). This would require a method for numerically solving a boundary value problem, from which one would find a very good approximation for the absorber response. This issue is explored further in the final chapter of the thesis.

2.2 Experimental Setup and Methods

In this section we first describe the experimental setup and equipments required for the experiments, and then describe the methods used to obtain the estimated absorber response from experiments.

2.2.1 Experimental Rig

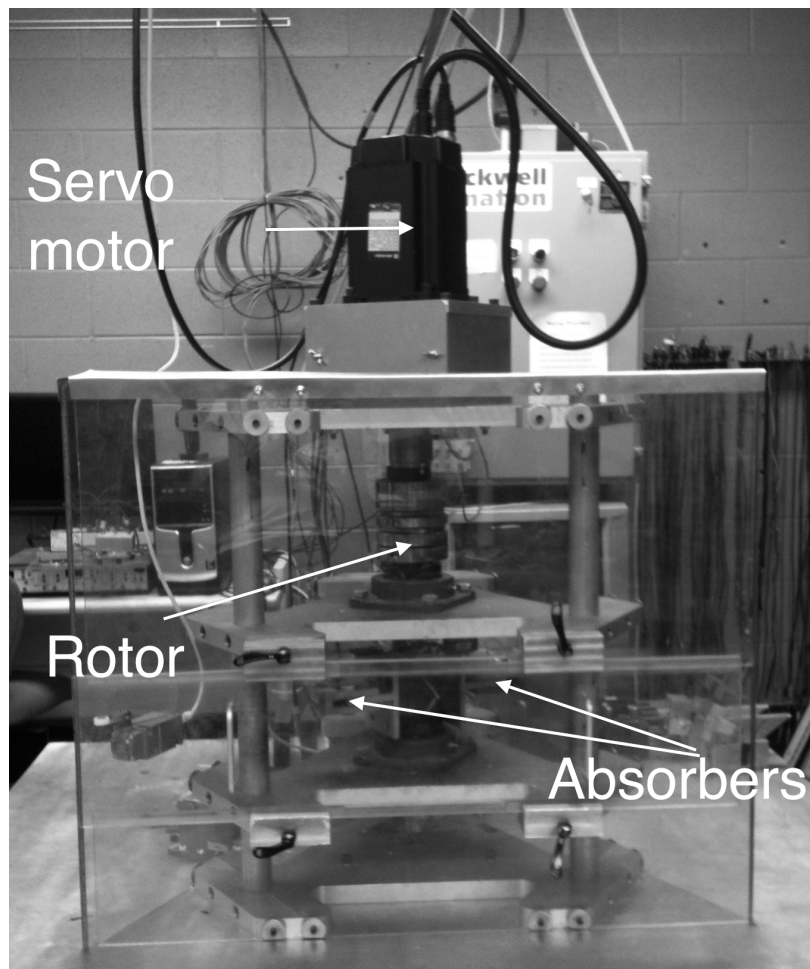


Figure 2.8: Experimental rig.

The experiments were performed using the existing rotor rig shown in Figure 2.8. This rig is described in detail in [9, 12]. It consists of a vertical shaft that is driven by a servo motor. The servo motor is controlled through a control system that takes its input from a

LabViewTM program.

The servo motor can be instructed through the program to run at a desired mean rotor speed Ω using a DC torque. An oscillating torque can be superimposed on the DC torque, resulting in torsional oscillations. The program allows for engine order excitation that mimics many applications, including automotive engines. The rig is designed to hold up to four torsional absorbers, but in the present study a single absorber is employed. The rotor dynamics ($\dot{\theta}$) are measured through data captured by an encoder. The absorber used in this study is shown in Figure 2.9. The absorber is mounted onto the rig using a pair of rollers. The absorber and encoder can be locked to the rotor (for reference measurements) or free to oscillate, in which case the angular displacement of the absorber relative to the rotor is measured using an encoder, as shown in Figure 2.9. In the bifilar case, it has been shown that the output of the encoder is nearly exactly proportional to the S displacement of the absorber, even out to large amplitudes [13]. The output from this encoder provides a measurement of the absorber motion that is independent of the accelerometer measurement, allowing for a means of validating the approach developed in this work.

2.2.2 Accelerometer Arrangement

Accelerometers measure absolute acceleration along certain predefined axes, x and y as shown in Figure 2.5, relative to the accelerometer. We measure the absolute acceleration of the absorbers using accelerometers by mounting them directly on the absorbers in such an orientation that the x and y axes of the accelerometer (see Figure 2.5) are aligned with the desired axes on the absorber, namely, \hat{e}_L and \hat{e}_ϕ for hinged absorbers (Figure 2.1) and \hat{e}_θ and \hat{e}_R for bifilar absorbers (Figure 2.2). Figure 2.9 shows an unmounted absorber mass, with

accelerometer and encoder mounted. The accelerometer is mounted on the absorber using super glue. To avoid surface damage of the absorber, the absorber is covered with masking tape and the accelerometer is mounted on the masking tape as shown in Figure 2.9.

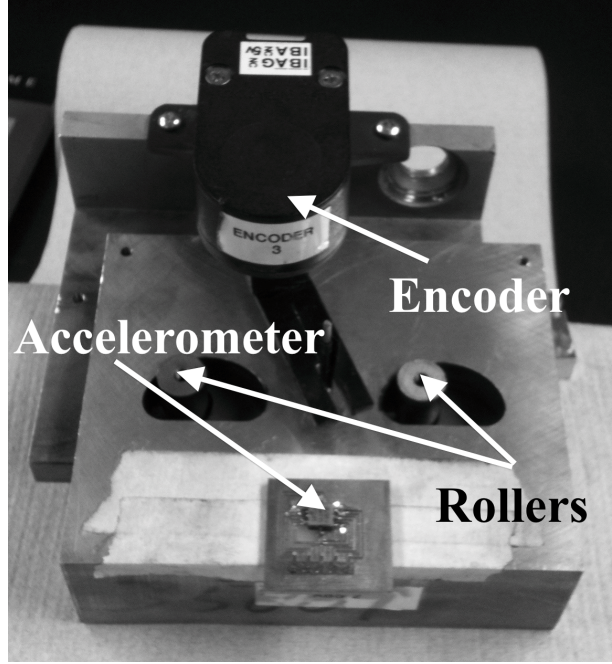


Figure 2.9: Closeup of unmounted absorber mass, with accelerometer and encoder.

2.2.3 System Parameter Values

To demonstrate the present method, we need to compare the expressions for acceleration from Equations (2.18) and (2.19) with the corresponding measured harmonics obtained from the accelerometer during experiment, from which the absorber response, given by P or S , can be determined. The quantities needed for the calculations are the distance c of the absorber COM from the rotor axis, the coefficients X_i 's and Y_i 's as given in Equation (2.12), and the accelerometer offset values δ_x and δ_y .

The distance c is measured using a vernier caliper. In our experimental setup, the rotor is cylindrical and thus, for convenience and accuracy, the distance from the further edge of

the rotor to the absorber COM ($c + r$) is noted and then the radius of rotor r is deducted from this measured value (see Figure 2.10). The accelerometer offsets δ_x and δ_y are also measured using a vernier caliper.

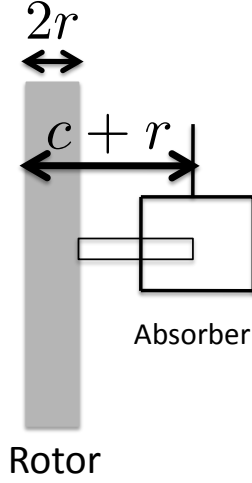


Figure 2.10: Procedure to measure the absorber COM distance from the rotor center.

The coefficients X_i and Y_i for the bifilar absorber have been derived from the exact expressions for $X(s)$ and $Y(s)$, as given in [6]. These coefficients, up to the cubic order are as follows,

$$X_1 \cong 1 \quad (2.22)$$

$$X_3 \cong -\frac{1}{6\rho_0^2} \quad (2.23)$$

$$Y_0 \cong c \quad (2.24)$$

$$Y_2 \cong -\frac{1}{2\rho_0} \quad (2.25)$$

where ρ_0 is the radius of curvature of the absorber at its vertex. It is determined using the

value of absorber tuning \tilde{n} (measured as described below) and distance c as follows [5, 6],

$$\rho_0 = \frac{c}{1 + \tilde{n}^2} \quad (2.26)$$

The parameters R and L for hinged absorbers can also be estimated distance c and the absorber tuning \tilde{n} using [5, 6, 7],

$$L = \frac{c}{1 + \tilde{n}^2} \quad (2.27)$$

$$R = c - L \quad (2.28)$$

To determine these values, we need to estimate the absorber tuning order \tilde{n} . The absorbers are designed to be tuned to a certain order, but one can experimentally verify the actual absorber tuning order. It can be shown [11] that the steady-state amplitude of the rotor angular acceleration, will have a minimum at \tilde{n} as the excitation order while n is varied. Shown in Figure 2.11 is the amplitude of the order n harmonic of the rotor angular acceleration normalized by the measured amplitude of the order n applied order torque versus the excitation order n . The tuning order estimated from this experiment is $\tilde{n} \approx 2.31$.

It should be noted that the absorber tuning will be affected by the placement of the accelerometers with respect to the absorber COM, and the accelerometer mass relative to the absorber mass. If δ_y is the offset of the accelerometer mass and m_a is the mass of accelerometer, the COM of the absorber will move from its original position due to the

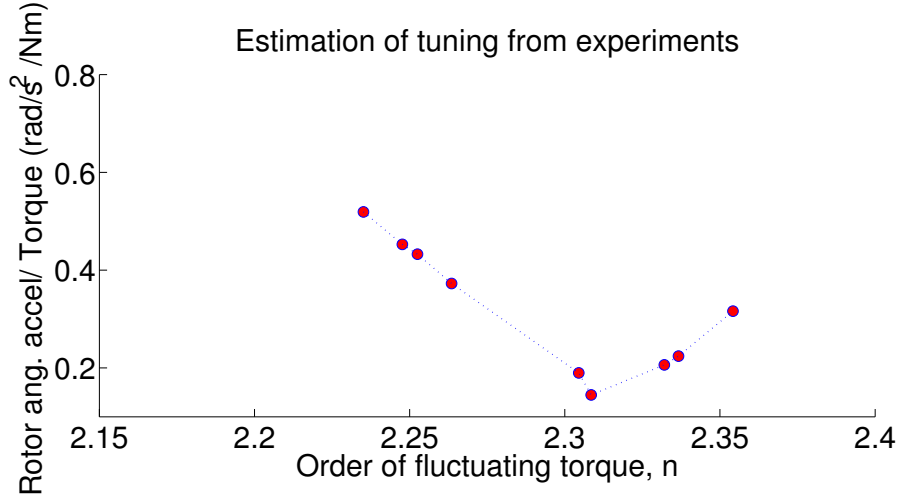


Figure 2.11: Order n amplitude of the rotor angular acceleration divided by the amplitude of fluctuating torque as a function of the applied torque order, n .

attachment of the accelerometer by Δ , given by

$$\Delta = \frac{m_a \delta_y}{m_p + m_a} \quad (2.29)$$

where m_p is the mass of the absorber. With this deviation in the location of the absorber COM, the absorber tuning order becomes \tilde{n}' , given by

$$\tilde{n}' = \frac{\tilde{n}}{\sqrt{1 + \frac{\Delta}{\rho_0}}} \quad (2.30)$$

where ρ_0 is the original radius of curvature of the absorber path at the vertex. In our system \tilde{n} and \tilde{n}' differ by $\Delta\tilde{n} \cong 0.336\%$, given by

$$\Delta\tilde{n} = \frac{|\tilde{n}' - \tilde{n}|}{\tilde{n}} * 100 \quad (2.31)$$

The resulting parameter values measured and estimated from experiments are summarized in Table 2.1

Table 2.1: **Parameter Values for Experiments**

Rotor center to absorber COM (c)	0.123 m
Absorber tuning (\tilde{n})	2.31
Radius of curvature at vertex (ρ_0)	0.0196
Accelerometer offset (δ_x)	0.000 m
Accelerometer offset (δ_y)	0.025 m
Absorber mass (m_p)	0.432 kg
Accelerometer mass (m_a)	0.0023 kg

The corresponding values for X_i and Y_i are obtained using the parameter values listed in Table 2.1 and Equations (2.22-2.25).

In order to simulate the dynamics equations of motion that correspond to the experimental conditions, we require additional dynamic parameters including the rotor inertia J , the absorber mass m_p , the rotor damping c_0 , and the absorber damping ratio μ_a . The dynamic parameters required for simulation are measured and estimated as given in [1] and are listed in Table 2.2.

Table 2.2: **Parameter Values for Dynamic Simulations [1]**

Parameter	Value
Absorber mass (m_p)	0.4312 kg
Rotor inertia (J)	0.01075 kg-m ²
Absorber viscous damping (μ_a)	0.105
Rotor damping (c_0)	0 .0144 Nms

2.3 Results

This section describes results obtained from the proposed method, for both simulations and experiments.

2.3.1 Simulations

The above sections outline a method for mapping data from an absorber-mounted accelerometer and a rotor encoder into the amplitude and phase of the absorber motion relative to the rotor. Before considering experimental data, the method is tested using simulation data. Since this is a purely kinematic exercise, it is possible to examine the method using some prescribed motions for the rotor and absorber and compute the resulting absorber acceleration components. However, in order to mimic the experimental procedure, the motions are computed using numerical integration of the known equations of motion for the rotor-absorber system, which are well known and can be found in [6, 7, 8, 9]. The typical outputs from the simulation are the rotor response ($\dot{\theta}$) and the absorber motion (ϕ or s). The components of absolute acceleration, which would be measured by an accelerometer in an experiment, need to be constructed from simulation data of $\dot{\theta}$ and ϕ or s , and their derivatives, using equations (2.4) and (2.8). In order to test the results based on the linear and cubic approximations, the signals from the acceleration and the rotor response are Fourier decomposed, keeping a single harmonic for the acceleration component of interest (a_ϕ or a_θ) and three harmonics for the rotor response. This filters out noise and provides the harmonic coefficients that are used to determine the complex amplitude of the first harmonic of the relative absorber motion.

The estimated data from the linear and cubic approximations are then plotted along

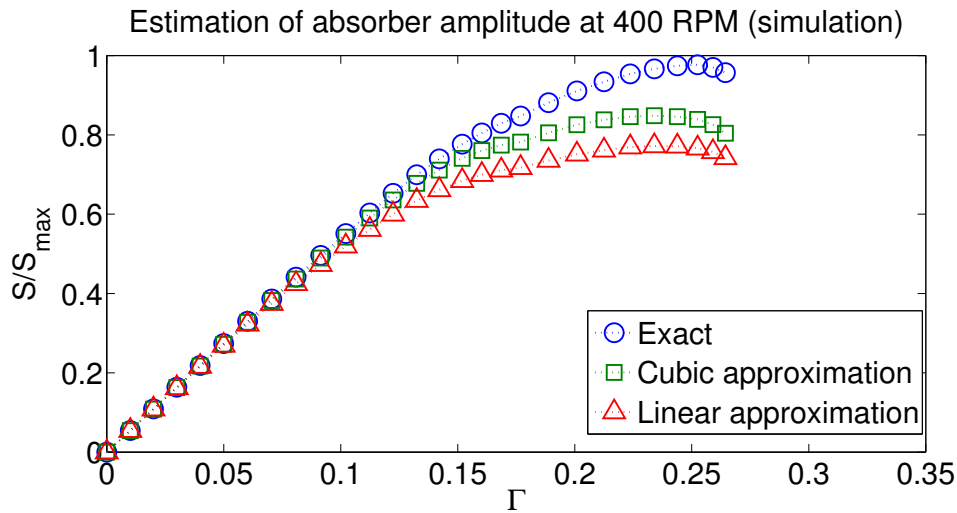


Figure 2.12: Normalized absorber displacement amplitude estimated from linear (Δ) and cubic (\square) analysis compared with exact values (\circ) at 400 RPM, over a range of absorber response amplitudes.

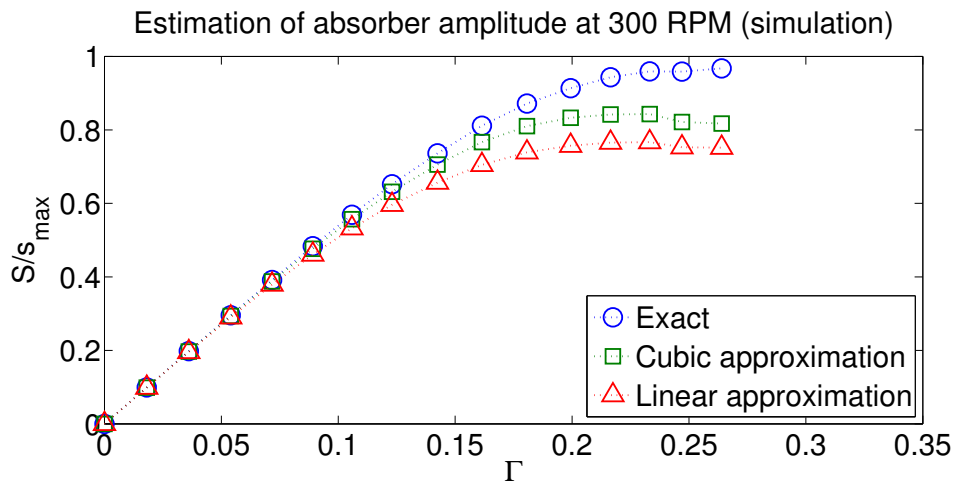


Figure 2.13: Normalized absorber displacement amplitude estimated from linear (Δ) and cubic (\square) analyses compared with exact values (\circ) at 300 RPM, over a range of absorber response amplitudes.

with the reference results obtained directly from simulations. The resulting plots are shown in Figure 2.12. Figures 2.12 and 2.13 shows result obtained from simulations of a bifilar absorber moving along a tautochronic epicycloidal path [8] with the rotor running at a mean speed of $\Omega = 400$ and 300 rpm respectively. The simulations were performed at a

low speed since we intend to compare it with experiments, which are also performed at low speeds due to the hardware constraints of the experimental rig. The scaled amplitude of the oscillating torque applied to the rotor varies along the horizontal axis and the corresponding absorber response is plotted along the vertical axis. The absorber response in the plot is the non-dimensional absorber amplitude $\frac{S}{S_{max}}$ which corresponds to the absorber amplitude normalized by the maximum amplitude the absorber can achieve (S_{max} is set by the cusp of the epicyloid [5]). The scaled oscillating torque amplitude is a non-dimensional quantity Γ , which corresponds to the ratio of the oscillating torque to twice the rotor kinetic energy, i.e., $\Gamma = \frac{|T|}{J\Omega^2}$. The plot shows three different curves, representing the absorber amplitude obtained in three different ways. The (\circ) curve represents the solutions from numerical simulations of EOM of the CPVA system. This data is analogous to the measured and filtered amplitude of the absorber obtained directly from the absorber encoders in the laboratory. The (\square) and (\triangle) curves represent estimated values of the absorber amplitude from the cubic (equation (2.14), appendix A.2.2) and linear (equation (2.21)) approximations, respectively. The result in Figure 2.12 shows that the predictions from the analysis are accurate when compared with the exact results from simulations for a moderate range of absorber amplitudes, say up to 60% of the cusp value. The approximate results begin to deviate from the simulation data at large absorber amplitudes, higher than 60% of the cusp value. The errors grow at a higher rate for estimations using the linear approximation as compared to estimations using the cubic approximation. This deviation is due to the Taylor series and finite harmonic assumptions used to approximate the non-linear system dynamics. Of course, one could improve the method by including more terms in the approximations. However, a more reasonable approach is to numerically find solutions of the differential equations for a_ϕ or

a_θ , which is discussed in the final chapter of this thesis. We now experimentally examine the proposed method.

2.3.2 Experimental Results

The absorber response that is estimated from the accelerometer and rotor encoder data using the present method will be compared to the absorber response taken directly from the absorber encoders. The response data is stored and post-processed using a LabViewTM program. The program computes the Fourier components of the signals taken from the accelerometer (for Θ_1), the rotor encoder (for Ω and the Q_i s), and the absorber encoder (for verification). The known and measured quantities are used as follows: For the linear approximation, they are substituted into equation (2.21) and solved in close form for S_r and S_j . For the cubic approximation, they are substituted into equations (A.44 - A.45), which are solved numerically for S_r and S_j . The absorber encoder is used to generate the reference result, which is the amplitude of the order n harmonic of the directly measured absorber response.

Results for a range of absorber amplitudes are obtained by sweeping the amplitude of the oscillating part of the torque acting on the rotor. Runs were carried out at 300, 400 and 500 RPM. The results obtained from each sweep, using the linear and cubic approximations, as well as the reference results from the absorber encoder, are shown in Figures 2.14, 2.15 and 2.16. The trends are the same as those observed in the simulations. Here the linear approximation works well up to about 50% of the maximum absorber amplitude, and the cubic approximation works well at all amplitudes we were able to measure, that is, up to about 80% of the allowable absorber amplitude. This agreement validates the approach

derived in this thesis.

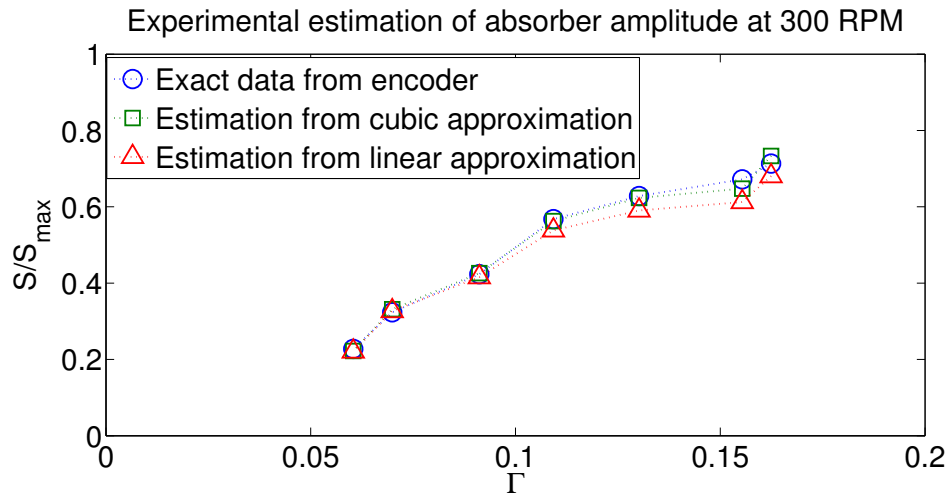


Figure 2.14: Absorber displacement amplitude S estimated from linear (\triangle) and cubic (\square) analyses compared with encoder values (\circ) at 300 RPM.

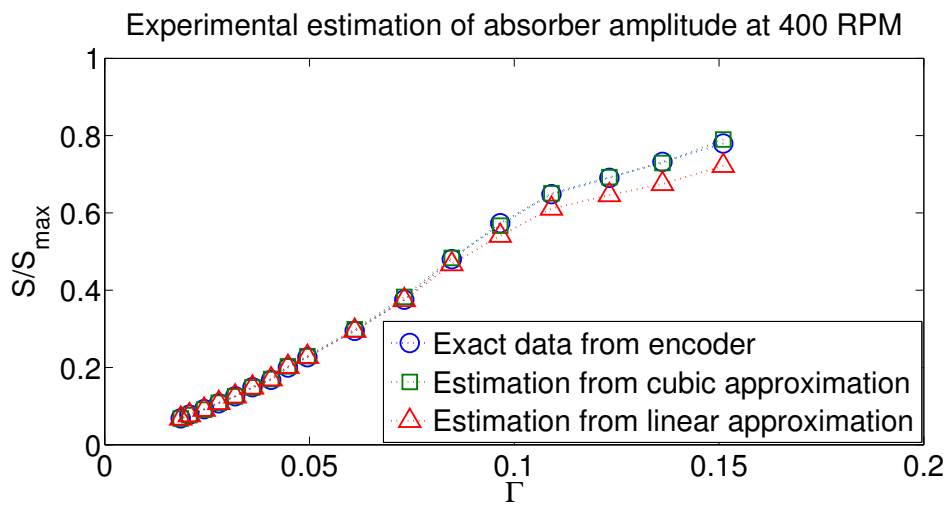


Figure 2.15: Absorber displacement amplitude S estimated from linear (\triangle) and cubic (\square) analyses compared with encoder values (\circ) at 400 RPM.

Figure 2.17 shows a comparison of the simulation and experimental results, both obtained using the cubic approximations. This comparison shows that the cubic estimation of the absorber response from simulations and experiments are in agreement up to about 80% of the peak absorber amplitude, which is at the limit of the experimental setup.

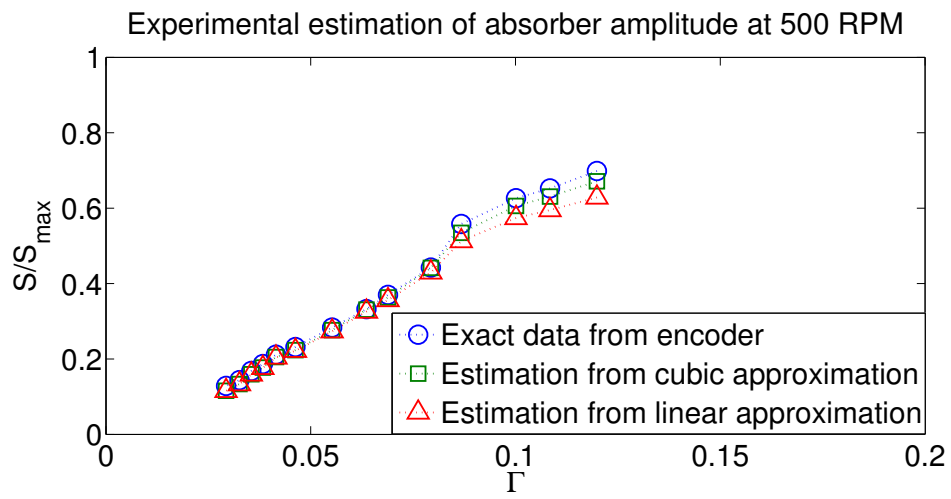


Figure 2.16: Absorber displacement amplitude S estimated from linear (\triangle) and cubic (\square) analyses compared with encoder values (\circ) at 500 RPM.

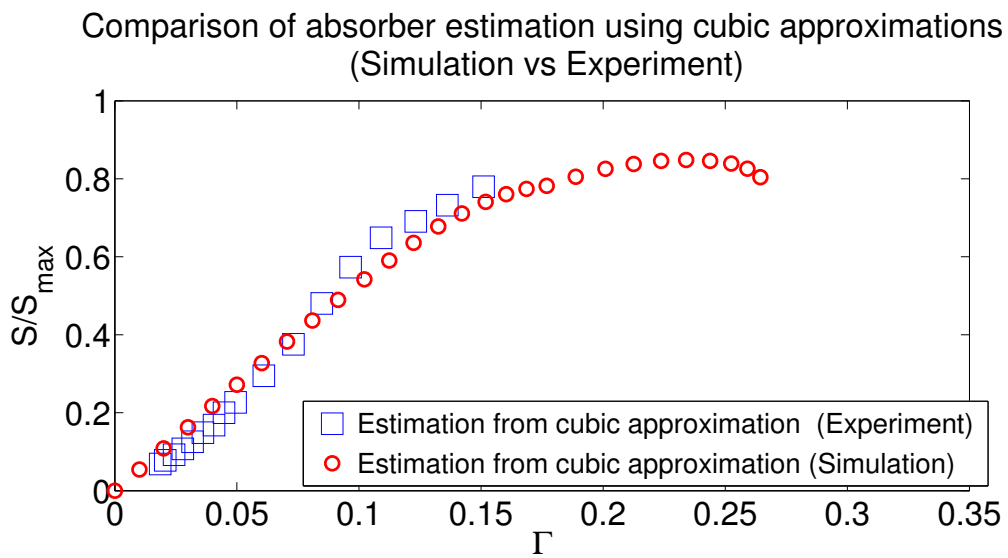


Figure 2.17: Comparison of cubic estimation from simulations and experiments.

Chapter 3

Conclusions and Future Work

The results generated from simulations as well as from experiments support the proposed method, of using an absorber-mounted accelerometer, as an effective means of determining the response of a centrifugal pendulum absorber in a running machine. The approximations developed are very good at low and moderate absorber amplitudes, but degrade at large amplitudes, due to the truncated nonlinear expansions and the approximations made in the harmonic balance analysis.

The proposed approach offers the benefit of small packaging space, and the potential for using telemetry [3] for data transfer, makes it appealing for applications. The main use of this approach will be in the development and testing of passive absorber systems, but it could also be used for active or semi-active pendulum absorber systems.

The present study provides a method for mapping the absorber acceleration into the information about the steady state response of the absorber. Some topics for improving and/or continuing this work include the following:

- (i) In our present analysis, we had assumed that the torque in the system is periodic with one harmonic. This method may be further modified and extended to include cases where the torque has multiple harmonics.
- (ii) The method can be generalized to the case of the transient response of absorbers in a

running system. In this case the issue of the initial conditions used in Equations (2.4) and (2.8) is crucial.

- (iii) This approach can also be extended to estimate the absorber damping using ring down tests. For this, a transformation of the absorber acceleration into a log decrement of the absorber response is required. Absorber damping is a key aspect in absorber performance and is often difficult to predict in a running engine. If we can propose a method of estimating the absorber damping coefficient using accelerometers, it will be important in the absorber design process.
- (iv) A detailed investigation of how uncertainties in measurements and the various approximations used affect the precision of the results would be beneficial for the understanding the limitations of the approach.
- (v) When absorbers are operated at large amplitudes, the linear approximation developed herein breaks down. One can use the cubic approximation, also described in this thesis, but it requires numerical solution of polynomial equations. If one is going to use numerical methods, it is probably worthwhile to deal more directly with the kinematic differential equations (2.4) and (2.8), and not resort to harmonic balance. Here we outline a proposed method for doing so for the case of bifilar absorbers; the approach for hinged absorbers is the same. For this direct approach, one would take measured signals for a_θ (from the accelerometer) and $\dot{\theta}$ (from the rotor encoder) and Fourier decompose each into a finite set of harmonics, essentially filtering these signals. These harmonic expressions would be used to generate the corresponding terms in equation (2.8), resulting in a second order ordinary differential equation for the unknown $S(t)$. The resulting equation has many time-periodic terms, both additive and multiplicative to

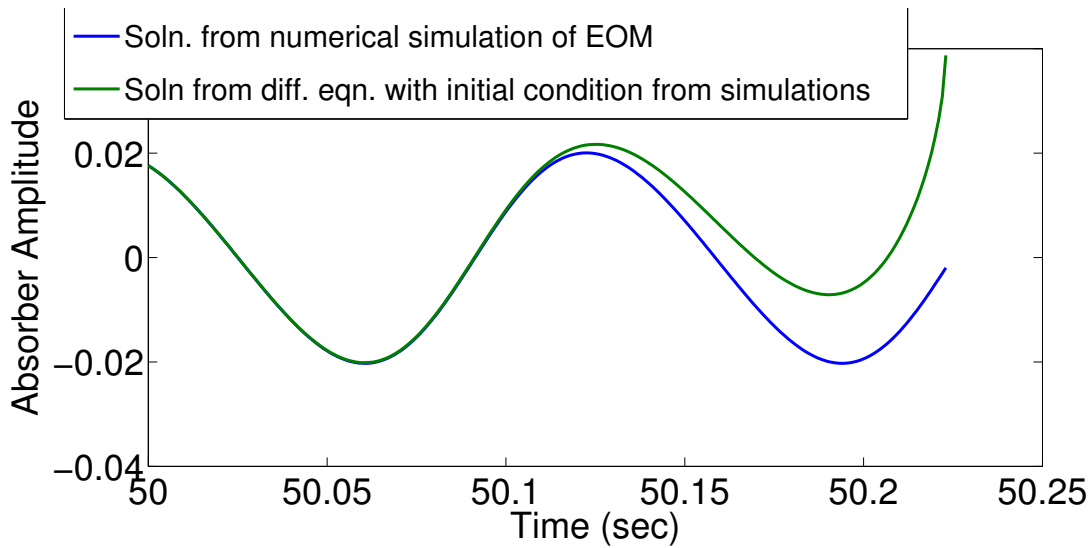


Figure 3.1: Comparison of simulated absorber dynamics with the numerical solution of differential equation (2.8).

S and its derivatives, and the unknown S appears through the known path functions $X(S)$ and $Y(S)$. The desired solution of this equation is time-periodic, and the initial conditions for this solution are unknown. It would be convenient if direct simulations of equation (2.8) with arbitrary initial conditions would settle onto this desired solution, but this is not the case. In fact, the desired solution is locally unstable. (Note that the periodic response of interest is dynamically stable, but here we are solving a purely kinematic equation.) Figure 3.1 shows two curves: the steady-state absorber response taken from direct simulations of the systems dynamics equations of motion (given in [7]), and a numerical solution of equation (2.8) obtained using initial conditions taken from the simulated response. In this case, the direct dynamic simulation provides all features of the periodic response $S(t)$ of interest to within small numerical errors, including the required initial conditions. By treating $S(t)$ as unknown in the corresponding kinematic differential equation (2.8), and using the correct initial conditions (to some finite precision), the solution of the kinematic equation should track the

desired solution. Figure 3.1 shows that it does so for a short time, but it quite quickly diverges from the desired periodic response, indicating its local instability. Therefore, one must formulate the solution of equation (2.8) as a boundary value problem and use numerical methods, for example, shooting methods, in order to obtain the desired solution. The resulting periodic solution will provide the desired absorber response relative to the rotor, from which its harmonic component at order n can be obtained. This is the recommended approach for large amplitude absorber motions.

- (vi) In fact, solutions of Equations (2.4) and (2.8) is central to all such studies, and a fundamental study of its properties would be of interest.

APPENDIX

Appendix A

Full Coefficients

A.1 Full Coefficients: Hinged Absorbers

From equation (2.16) we can write the absorber dynamics in terms of harmonics with complex coefficients P and P^* , where

$$P = P_r + iP_i \tag{A.1}$$

Similarly in equation (2.15), the individual coefficients Q_j can be written as

$$Q_j = (Q_{jr} + iQ_{ji}), \quad j = 1, 2, 3 \tag{A.2}$$

We substitute these values into equation (2.15), and then into the expression for a_ϕ in equation (2.13) to obtain a Fourier series, as given in equation (2.18). Since we are only interested in the Φ_1 term, we extract the first harmonic in complex form to obtain

$$\Phi_1 = \Phi_r + i\Phi_i \tag{A.3}$$

A.1.1 Linear Approximation

If we truncate equation (2.13) at linear terms in ϕ and substitute the expressions of P and Q in the linear expression, we get the Φ_r and Φ_i as

$$\Phi_r = f_1 P_r + f_2 P_i + c_1 \quad (\text{A.4})$$

$$\Phi_i = f_3 P_r + f_4 P_i + c_2$$

where f_1, f_2, f_3, f_4, c_1 and c_2 are as follows:

$$f_1 = R(2\Omega Q_{2i} + 2(Q_{1i} + Q_{3i})Q_{1r} - n\Omega Q_{2r} - 2Q_{1i}Q_{3r}) + 2n\Omega(-\Omega + Q_{2r})\delta_x \quad (\text{A.5})$$

$$\begin{aligned} f_2 = & \left(-Ln^2 + R\right)\Omega^2 + 3RQ_{1i}^2 + 2RQ_{2i}^2 - 2RQ_{1i}Q_{3i} + \\ & R\left(2Q_{3i}^2 + Q_{1r}^2 + 2Q_{2r}(-\Omega + Q_{2r}) - 2Q_{1r}Q_{3r} + 2Q_{3r}^2\right) - n\Omega Q_{2i}(R - 2\delta_x) - n^2\Omega^2\delta_y \end{aligned} \quad (\text{A.6})$$

$$\begin{aligned} f_3 = & \left(-Ln^2 + R\right)\Omega^2 + RQ_{1i}^2 + 2RQ_{2i}^2 + 2RQ_{1i}Q_{3i} + \\ & R\left(2Q_{3i}^2 + 3Q_{1r}^2 + 2Q_{2r}(\Omega + Q_{2r}) + 2Q_{1r}Q_{3r} + 2Q_{3r}^2\right) + n\Omega Q_{2i}(R - 2\delta_x) - n^2\Omega^2\delta_y \end{aligned} \quad (\text{A.7})$$

$$f_4 = R(2\Omega Q_{2i} + 2(Q_{1i} + Q_{3i})Q_{1r} - n\Omega Q_{2r} - 2Q_{1i}Q_{3r}) + 2n\Omega(\Omega + Q_{2r})\delta_x \quad (\text{A.8})$$

$$c_1 = 2(-\Omega Q_{1i} + (Q_{1i} - Q_{3i})Q_{2r} + Q_{2i}Q_{3r})\delta_x + Q_{1r}(-2Q_{2i}\delta_x + n\Omega(L + R + \delta_y)) \quad (\text{A.9})$$

$$c_2 = -2(Q_{2i}Q_{3i} + Q_{1r}(\Omega + Q_{2r}) + Q_{2r}Q_{3r})\delta_x - Q_{1i}(2Q_{2i}\delta_x + n\Omega(L + R + \delta_y)) \quad (\text{A.10})$$

Using equations (A.5) to (A.10) we can obtain the amplitude of absorber P in closed form as shown in equation (2.20)

$$\begin{aligned} P_r &= \frac{(\Phi_r - c_1) f_4 - (\Phi_i - c_2) f_2}{f_1 f_4 - f_2 f_3} \\ P_i &= \frac{(\Phi_r - c_1) f_3 - (\Phi_i - c_2) f_1}{f_2 f_3 - f_4 f_1} \end{aligned} \quad (\text{A.11})$$

A.1.2 Cubic Approximation

Substituting equations (A.1) and (A.2) into the cubic expression of equation (2.13), we get expression for Φ_r and Φ_i as follows:

$$\begin{aligned} \Phi_r &= c_{00} + c_{10}P_r + c_{20}P_r^2 + c_{30}P_r^3 + c_{11}P_rP_i + \\ &\quad c_{12}P_rP_i^2 + c_{21}P_r^2P_i + c_{01}P_i + c_{02}P_i^2 + c_{03}P_i^3 \end{aligned} \quad (\text{A.12})$$

$$\begin{aligned} \Phi_i &= d_{00} + d_{10}P_r + d_{20}P_r^2 + d_{30}P_r^3 + d_{11}P_rP_i + \\ &\quad d_{12}P_rP_i^2 + d_{21}P_r^2P_i + d_{01}P_i + d_{02}P_i^2 + d_{03}P_i^3 \end{aligned} \quad (\text{A.13})$$

where the values of coefficients c_{ii} and d_{ii} are as follows:

$$c_{00} = c_1 \quad (\text{A.14})$$

$$c_{10} = f_1 \quad (\text{A.15})$$

$$c_{20} = 0 \quad (\text{A.16})$$

$$c_{30} = -\frac{1}{3}R(3Q_{3i}Q_{1r} + Q_{2i}(2\Omega + Q_{2r}) + Q_{1i}(2Q_{1r} - Q_{3r})) \quad (\text{A.17})$$

$$c_{11} = 0 \quad (\text{A.18})$$

$$c_{12} = R(-(2Q_{1i} + Q_{3i})Q_{1r} + Q_{2i}(-2\Omega + Q_{2r}) + 3Q_{1i}Q_{3r}) \quad (\text{A.19})$$

$$c_{21} = -\frac{1}{2}R\left(\Omega^2 + 3Q_{2i}^2 + 2\left(Q_{1i}^2 + Q_{1i}Q_{3i} + Q_{3i}^2\right) + Q_{2r}^2 + 2\left(Q_{1r}^2 - Q_{1r}Q_{3r} + Q_{3r}^2\right)\right) \quad (\text{A.20})$$

$$c_{01} = f_2 \quad (\text{A.21})$$

$$c_{02} = 0 \quad (\text{A.22})$$

$$c_{03} = -\frac{1}{6}R\left(3\Omega^2 + 10Q_{1i}^2 + 5Q_{2i}^2 - 10Q_{1i}Q_{3i}\right) + \frac{1}{6}\left(6Q_{3i}^2 + 2Q_{1r}^2 - 8\Omega Q_{2r} + 7Q_{2r}^2 - 6Q_{1r}Q_{3r} + 6Q_{3r}^2\right) \quad (\text{A.23})$$

$$d_{00} = c_2 \quad (\text{A.24})$$

$$d_{10} = f_3 \quad (\text{A.25})$$

$$d_{20} = 0 \quad (\text{A.26})$$

$$d_{30} = -\frac{1}{6}R\left(3\Omega^2 + 2Q_{1i}^2 + 5Q_{2i}^2 + 6Q_{1i}Q_{3i}\right) + \frac{1}{6}\left(6Q_{3i}^2 + 10Q_{1r}^2 + 8\Omega Q_{2r} + 7Q_{2r}^2 + 10Q_{1r}Q_{3r} + 6Q_{3r}^2\right) \quad (\text{A.27})$$

$$d_{11} = 0 \quad (\text{A.28})$$

$$d_{12} = -\frac{1}{2}R \left(\Omega^2 + 3Q_{2i}^2 + 2 \left(Q_{1i}^2 + Q_{1i}Q_{3i} + Q_{3i}^2 \right) + Q_{2r}^2 + 2 \left(Q_{1r}^2 - Q_{1r}Q_{3r} + Q_{3r}^2 \right) \right) \quad (\text{A.29})$$

$$d_{21} = -R (3Q_{3i}Q_{1r} + Q_{2i} (2\Omega + Q_{2r}) + Q_{1i} (2Q_{1r} - Q_{3r})) \quad (\text{A.30})$$

$$d_{01} = f_4 \quad (\text{A.31})$$

$$d_{02} = 0 \quad (\text{A.32})$$

$$d_{03} = -\frac{1}{3}R \left(-(2Q_{1i} + Q_{3i}) Q_{1r} + Q_{2i} (-2\Omega + Q_{2r}) + 3Q_{1i}Q_{3r} \right) \quad (\text{A.33})$$

A.2 Full Coefficients: Bifilar Absorbers

Using a similar approach, as in section A.1.1 with hinged absorbers we can write the order n harmonic coefficient of S as follows

$$S = S_r + iS_i \quad (\text{A.34})$$

The rotor harmonics are expressed as given in equation (A.2). We substitute these expressions into equation (2.14) and carry out a Fourier expansion. Since we are only interested in the Θ_1 term, we retain the first harmonic from the expression obtained by the substitution of equation (A.34) and (A.2) into (2.19) to obtain

$$\Theta_1 = \Theta_r + \Theta_i \quad (\text{A.35})$$

A.2.1 Linear Approximation

If we truncate equation (2.14) to include only linear terms in θ and substitute the expressions of S and Q into the linear expression, we get the Θ_r and Θ_i as

$$\begin{aligned}\Theta_r &= F_1 S_r + F_2 S_i + C_1 \\ \Theta_i &= F_3 S_r + F_4 S_i + C_2\end{aligned}\tag{A.36}$$

where F_1, F_2, F_3, F_4, C_1 and C_2 are given by

$$\begin{aligned}F_1 &= - \left((1 + n^2) \Omega^2 + Q_{1i}^2 + 2Q_{2i}^2 + 2Q_{1i}Q_{3i} \right) X_1 - \\ &\quad \left(2Q_{3i}^2 + 3Q_{1r}^2 + 2Q_{2r}(\Omega + Q_{2r}) + 2Q_{1r}Q_{3r} + 2Q_{3r}^2 \right) X_1\end{aligned}\tag{A.37}$$

$$F_2 = -2(\Omega Q_{2i} + (Q_{1i} + Q_{3i})Q_{1r} - Q_{1i}Q_{3r})X_1\tag{A.38}$$

$$F_3 = -F_2\tag{A.39}$$

$$\begin{aligned}F_4 &= - \left((1 + n^2) \Omega^2 + 3Q_{1i}^2 + 2Q_{2i}^2 - 2Q_{1i}Q_{3i} \right) X_1 + \\ &\quad \left(2Q_{3i}^2 + Q_{1r}^2 + 2Q_{2r}(-\Omega + Q_{2r}) - 2Q_{1r}Q_{3r} + 2Q_{3r}^2 \right) X_1\end{aligned}\tag{A.40}$$

$$\begin{aligned}C_1 &= -2(Q_{2i}Q_{3i} + Q_{1r}(\Omega + Q_{2r}) + Q_{2r}Q_{3r})\delta_X + \\ &\quad Q_{1i}(2Q_{2i}\delta_X + n\Omega(Y_0 + \delta_Y))\end{aligned}\tag{A.41}$$

$$C_2 = 2(-\Omega Q_{1i} + (Q_{1i} - Q_{3i}) Q_{2r} + Q_{2i} Q_{3r}) \delta_X + Q_{1r} (-2Q_{2i} \delta_X + n\Omega (Y_0 + \delta_Y)) \quad (\text{A.42})$$

where $X_1 = 1$, $X_3 = -\frac{1}{6\rho_0^2}$, $Y_0 = c$, $Y_2 = -\frac{1}{2\rho_0}$ and ρ_0 is the radius of curvature of the absorber COM path at the vertex.

Using equations (A.37) to (A.42) we can obtain the amplitude of absorber P in closed form as shown in equation (2.21).

$$\begin{aligned} S_r &= \frac{(\Theta_r - C_1) F_4 - (\Theta_i - C_2) F_2}{F_1 F_4 - F_2 F_3} \\ S_i &= \frac{(\Theta_r - C_1) F_3 - (\Theta_i - C_2) F_1}{F_2 F_3 - F_4 F_1} \end{aligned} \quad (\text{A.43})$$

A.2.2 Cubic Approximation

Similar to the cubic expressions developed for hinged absorbers in Appendix A.1.2 , we can develop a cubic approximation of equation (2.14), resulting in expressions for Θ_r and Θ_i as

$$\begin{aligned} \Theta_r &= a_{00} + a_{10} S_r + a_{20} S_r^2 + a_{30} S_r^3 + a_{11} S_r S_i + \\ & a_{21} S_r^2 S_i + a_{12} S_r S_i^2 + a_{01} S_i + a_{02} S_i^2 + a_{03} S_i^3 \end{aligned} \quad (\text{A.44})$$

$$\begin{aligned} \Theta_i &= b_{00} + b_{10} S_r + b_{20} S_r^2 + b_{30} S_r^3 + b_{11} S_r S_i + \\ & b_{21} S_r^2 S_i + b_{12} S_r S_i^2 + b_{01} S_i + b_{02} S_i^2 + b_{03} S_i^3 \end{aligned} \quad (\text{A.45})$$

where the values of coefficient a_{ii} and b_{ii} are as follows:

$$a_{00} = C_1 \quad (\text{A.46})$$

$$a_{10} = F_1 \quad (\text{A.47})$$

$$a_{20} = n\Omega (Q_{1i} + Q_{3i}) Y_2 \quad (\text{A.48})$$

$$\begin{aligned} a_{30} = & - \left(3 \left(1 + n^2 \right) \Omega^2 + 2Q_{1i}^2 + 5Q_{2i}^2 + 6Q_{1i}Q_{3i} \right) X_3 - \\ & \left(6Q_{3i}^2 + 10Q_{1r}^2 + Q_{2r} (8\Omega + 7Q_{2r}) \right) X_3 - \\ & \left(10Q_{1r}Q_{3r} + 6Q_{3r}^2 \right) X_3 \quad (\text{A.49}) \end{aligned}$$

$$a_{11} = -2n\Omega (3Q_{1r} + Q_{3r}) Y_2 \quad (\text{A.50})$$

$$\begin{aligned} a_{12} = & -3 \left(\left(1 + n^2 \right) \Omega^2 + 3Q_{2i}^2 \right) X_3 - \\ & 3 \left(2 \left(Q_{1i}^2 + Q_{1i}Q_{3i} + Q_{3i}^2 \right) + Q_{2r}^2 \right) X_3 - \\ & 3 \left(2 \left(Q_{1r}^2 - Q_{1r}Q_{3r} + Q_{3r}^2 \right) \right) X_3 \quad (\text{A.51}) \end{aligned}$$

$$a_{21} = -6 (3Q_{3i}Q_{1r} + Q_{2i} (2\Omega + Q_{2r}) + Q_{1i} (2Q_{1r} - Q_{3r})) X_3 \quad (\text{A.52})$$

$$a_{01} = F_2 \quad (\text{A.53})$$

$$a_{02} = -n\Omega (5Q_{1i} + Q_{3i}) Y_2 \quad (\text{A.54})$$

$$a_{03} = -2 \left((2Q_{1i} + Q_{3i}) Q_{1r} + Q_{2i} (2\Omega - Q_{2r}) - 3Q_{1i}Q_{3r} \right) X_3 \quad (\text{A.55})$$

$$b_{00} = C_2 \quad (\text{A.56})$$

$$b_{10} = F_3 \quad (\text{A.57})$$

$$b_{20} = n\Omega (5Q_{1r} - Q_{3r}) Y_2 \quad (\text{A.58})$$

$$b_{30} = -2 (3Q_{3i}Q_{1r} + Q_{2i} (2\Omega + Q_{2r}) + Q_{1i} (2Q_{1r} - Q_{3r})) X_3 \quad (\text{A.59})$$

$$b_{11} = 2n\Omega (3Q_{1i} - Q_{3i}) Y_2 \quad (\text{A.60})$$

$$b_{12} = -6 ((2Q_{1i} + Q_{3i}) Q_{1r} + Q_{2i} (2\Omega - Q_{2r}) - 3Q_{1i}Q_{3r}) X_3 \quad (\text{A.61})$$

$$b_{21} = -3 \left((1 + n^2) \Omega^2 + 3Q_{2i}^2 \right) X_3 -$$

$$3 \left(2 \left(Q_{1i}^2 + Q_{1i}Q_{3i} + Q_{3i}^2 \right) + Q_{2r}^2 \right) X_3 -$$

$$3 \left(2 \left(Q_{1r}^2 - Q_{1r}Q_{3r} + Q_{3r}^2 \right) \right) X_3 \quad (\text{A.62})$$

$$b_{01} = F_4 \quad (\text{A.63})$$

$$b_{02} = n\Omega (-Q_{1r} + Q_{3r}) Y_2 \quad (\text{A.64})$$

$$b_{03} = - \left(3 (1 + n^2) \Omega^2 + 10Q_{1i}^2 \right) X_3 -$$

$$\left(5Q_{2i}^2 - 10Q_{1i}Q_{3i} + 6Q_{3i}^2 + 2Q_{1r}^2 + Q_{2r} (-8\Omega + 7Q_{2r}) \right) X_3 +$$

$$\left(6Q_{1r}Q_{3r} - 6Q_{3r}^2 \right) X_3 \quad (\text{A.65})$$

BIBLIOGRAPHY

BIBLIOGRAPHY

- [1] Brendan James Vidmar. *Analysis and Design of Multiple Order Centrifugal Pendulum Vibration Absorbers*. PhD thesis, Michigan State University, 2012.
- [2] Tyler M. Nester, Alan Haddow, Steven W. Shaw, and et al. Vibration reduction in a variable displacement engine using pendulum absorbers, 2003.
- [3] Scott A. Meirs and et. al. A wireless microwave telemetry data transfer technique for reciprocating and rotating components.
- [4] J. Madden. Constant frequency bifilar vibration absorbers, 1980.
- [5] S.W. Shaw and B. Geist. Tuning for performance and stability in systems of nearly tautochronic torsional vibration absorbers.
- [6] H. H. Denman. Tautochronic bifilar pendulum torsion tautochronic bifilar pendulum torsion absorbers for reciprocating engines, 1992.
- [7] A.S. Alsuwaiyan. Performance and dynamic stability of general-path centrifugal pendulum vibration absorbers, 2002.
- [8] Ryan James Monroe. Nonlinear transient dynamics of pendulum torsional vibration absorbers—part - 1: Theory.
- [9] Ryan James Monroe. Nonlinear transient dynamics of pendulum torsional vibration absorbers — part - 2: Experimental results.
- [10] A.S. Alsuwaiyan. *Performance, Stability, and Localization of Systems of Vibration absorbers*. PhD thesis, Michigan State University, 1999.
- [11] A. G. Haddow and S. W. Shaw. Centrifugal pendulum vibration absorbers: An experimental and theoretical investigation. In *Nonlinear Dynamics*, 2003.
- [12] Brendan James Vidmar. The effects of coulomb friction on the performance of centrifugal pendulum vibration absorbers. In *Nonlinear Dynamics*, 2012.
- [13] S. W. Shaw, P. M. Schmitz, and A. G. Haddow. Tautochronic vibration absorber for rotating systems, 2006.